# Synthesis, pharmacological assessment, molecular modeling and in silico studies of fused tricyclic coumarin derivatives as a new family of multifunctional anti-Alzheimer agents

**ARTICLE** *in* EUROPEAN JOURNAL OF MEDICINAL CHEMISTRY · OCTOBER 2015

Impact Factor: 3.45 · DOI: 10.1016/j.ejmech.2015.10.046

European Journal of Medicinal Chemistry 107 (2016) 219–232

Contents lists available at ScienceDirect

European Journal of Medicinal Chemistry

journal homepage: http://www.elsevier.com/locate/ejmech

Research paper

# Synthesis, pharmacological assessment, molecular modeling and *in silico* studies of fused tricyclic coumarin derivatives as a new family of multifunctional anti-Alzheimer agents

Jeelan Basha Shaik [a], Bhagath Kumar Palaka [b], Mohan Penumala [a], Kasi Viswanath Kotapati [b], Subba Rao Devineni [c], Siddhartha Eadlapalli [d], M. Manidhar Darla [c], Dinakara Rao Ampasala [b], Ramakrishna Vadde [d], G. Damu Amooru [a, *]

[a] Department of Chemistry, Yogi Vemana University, Kadapa, India
[b] Centre for Bioinformatics, School of Life Sciences, Pondicherry Central University, Puducherry, India
[c] Department of Chemistry, University College of Sciences, Sri Venkateswara University, Tirupati, India
[d] Department of Biotechnology and Bioinformatics, Yogi Vemana University, Kadapa, India

ARTICLE INFO

*Article history:*
Received 15 July 2015
Received in revised form
23 October 2015
Accepted 28 October 2015
Available online 31 October 2015

*Keywords:*
Alzheimer's disease
Fused tricyclic coumarin
Antioxidant
Acetylcholinesterase
Butyrylcholinesterase
Neuroprotection
Molecular modeling study
ADMET

ABSTRACT

A series of fused tricyclic coumarin derivatives bearing iminopyran ring connected to various amido moieties were developed as potential multifunctional anti-Alzheimer agents for their cholinesterase inhibitory and radical scavenging activities. In vitro studies revealed that most of these compounds exhibited high inhibitory activity on acetylcholinesterase (AChE), with $IC_{50}$ values ranging from 0.003 to 0.357 μM which is 2–220 folds more potent than the positive control, galantamine. Their inhibition selectivity against AChE over butyrylcholinesterase (BuChE) has increased about 194 fold compared with galantamine. The developed compounds also showed potent ABTS radical scavenging activity ($IC_{50}$ 7.98 −15.99 μM). Specifically, the most potent AChE inhibitor **6n** ($IC_{50}$ 0.003 ± 0.0007 μM) has an excellent antioxidant profile as determined by the ABTS method ($IC_{50}$ 7.98 ± 0.77 μM). Moreover, cell viability studies in SK N SH cells showed that the compounds **6m**–**q** have significant neuroprotective effects against $H_2O_2$-induced cell death, and are not neurotoxic at all concentrations except **6n** and **6q**. The kinetic analysis of compound **6n** proved that it is a mixed-type inhibitor for *Ee*AChE ($K_{i1}$ 0.0103 μM and $K_{i2}$ 0.0193 μM). Accordingly, the molecular modeling study demonstrated that **6m**–**q** with substituted benzyl amido moiety possessed an optimal docking pose with interactions at catalytic active site (CAS) and peripheral anionic site (PAS) of AChE simultaneously and thereby they might prevent aggregation of Aβ induced by AChE. Furthermore, *in silico* ADMET prediction studies indicated that these compounds satisfied all the characteristics of CNS acting drugs. Most active inhibitor **6n** is permeable to BBB as determined in the *in vivo* brain AChE activity. To sum up, the multipotent therapeutic profile of these novel tricyclic coumarins makes them promising leads for developing anti-Alzheimer agents.



## 1. Introduction

Alzheimer's disease (AD) is a deadly neurodegenerative disorder that attacks the central nervous system through progressive degeneration of its neurons [1]. It is the most common form of dementia affecting over 35 million people worldwide. AD is characterized by the loss of memory, progressive and irreversible cognitive impairments, language deterioration, severe behavioral abnormalities, and ultimately causing death [2]. Despite AD has been found for more than a century, it is still incurable as its etiology has not yet been fully explored. However, low levels of acetylcholine (ACh), oxidative stress, the inflammation of neurons and β-amyloid (Aβ) deposits are thought to play definitive roles in AD pathogenesis. Based on these factors several hypotheses which include cholinergic and noncholinergic interventions have been emerged over the past decades [3]. However, the cholinergic

* Corresponding author.
*E-mail address:* agdamu01@gmail.com (G.D. Amooru).

http://dx.doi.org/10.1016/j.ejmech.2015.10.046
0223-5234/

hypothesis which enhances the central cholinergic function by maintaining ACh levels via inhibition of acetylcholinesterase (AChE) is the only approved therapeutic strategy for the treatment of AD.

Recently it has been shown that AChE involves in the extraneous non-cholinergic function in the early phases of AD by binding to Aβ, thereby accelerating its polymerization into oligomers and fibrils and increasing the neurotoxicity of Aβ aggregates [4,5]. The peripheral anionic site (PAS) has been shown to play a crucial role in Aβ pro-aggregating action of AChE. It is located at the mouth of a 20 Å deep gorge and leads to the catalytic anionic site (CAS) of the enzyme. Considering these aspects, AChE inhibitors that bind to either PAS or to both the CAS and PAS may simultaneously alleviate the cognitive deficit and delay the neurodegenerative process by preventing the assembly of Aβ-peptide [6–10].

Furthermore, inhibition of butyrylcholinesterase (BuChE), an enzyme closely related to AChE has been found to be a desirable activity in design of anti-Alzheimer agents [11]. However, serious inhibition of BuChE causes peripheral side effects including gastrointestinal events, nausea, vomiting, diarrhea and dizziness as it is mainly localized in the peripheral tissues including plasma and several regions of the brain. For example, the dual AChE and BuChE inhibitor, tacrine showed severe hepatotoxicity as well as other adverse effects and so withdrawn from the use. Therefore, the development of selective AChE inhibitors to reduce side effects may be a more suitable therapeutic strategy for the treatment of AD [12].

Increasing evidence supports the significant impact of oxidative stress in initiating the aggregation of Aβ and tau protein hyperphosphorylation, involved in the early stage of the pathologic cascade [13]. Oxidative cell damage marked by lipid peroxidation, nitration, reactive carbonyls, and nucleic acid oxidation is at higher level in vulnerable neurons in AD [14]. Thus, neuroprotection against oxidative stress induced cell damage in neuronal cells has become the important target for AD treatment. Therefore, the combination of selective AChEIs, antioxidants and neuroprotectives represents an additional rational approach to develop new multifunctional agents for AD treatment [15,16].

Naturally occurring and chemically synthesized coumarins have received intense attention in recent years because of their wide ranging biological activities [17]. Researchers have attempted to explore the coumarin template for developing novel AChE inhibitors with additional pharmacological activities such as decrease in Aβ deposition and β-secretase inhibition that are also important for AD management [18–21]. Coumarin derivatives have also been protecting neurons against Aβ-induced oxidative stress and free radicals [22,23]. Since coumarins primarily interact with PAS of AChE, several coumarin based dual inhibitors of AChE were designed by incorporating a catalytic site interacting moiety through an appropriate spacer [24–31]. As a result, the 3rd or 4th position of coumarin moiety has been described as the most favorable for linking CAS interacting moiety but not 6th or 7th to obtain potent dual site AChE inhibitors [18]. However, we focused our attention for the first time on angularly fused iminopyran at 7 and 8 positions of 7-hydroxy-4-methylcoumarin bearing various N-substituted amides on 9th position. Thus we report herein synthesis, biological evaluation, molecular modeling and *in silico* studies of a series of fused tricyclic coumarin amide derivatives as novel multifunctional anti-AD agents with potent and selective AChE over BuChE inhibitory and antioxidant activities.

## 2. Results and discussion

### 2.1. Chemistry

The synthetic pathway of fused tricyclic coumarins (**6a**–**s**) was outlined in Scheme 1. The target molecules consist of three parts, therefore the synthetic strategy involves the preparation of cyano acetamide derivative by reacting different amines with ethylcyanoacetate and then fused it to the formyl coumarin. At first, a series of N-substituted cyano acetamide derivatives (**2a**–**s**) were prepared by simple reaction in readily available screw cap bottle by treating amines with equivalent amount of ethylcyanoacetate [32,33]. Resorcinol (**3**) and ethylacetoacetate were treated under Pechmann conditions to give 7-hydroxy-4-methylcoumarin (**4**)

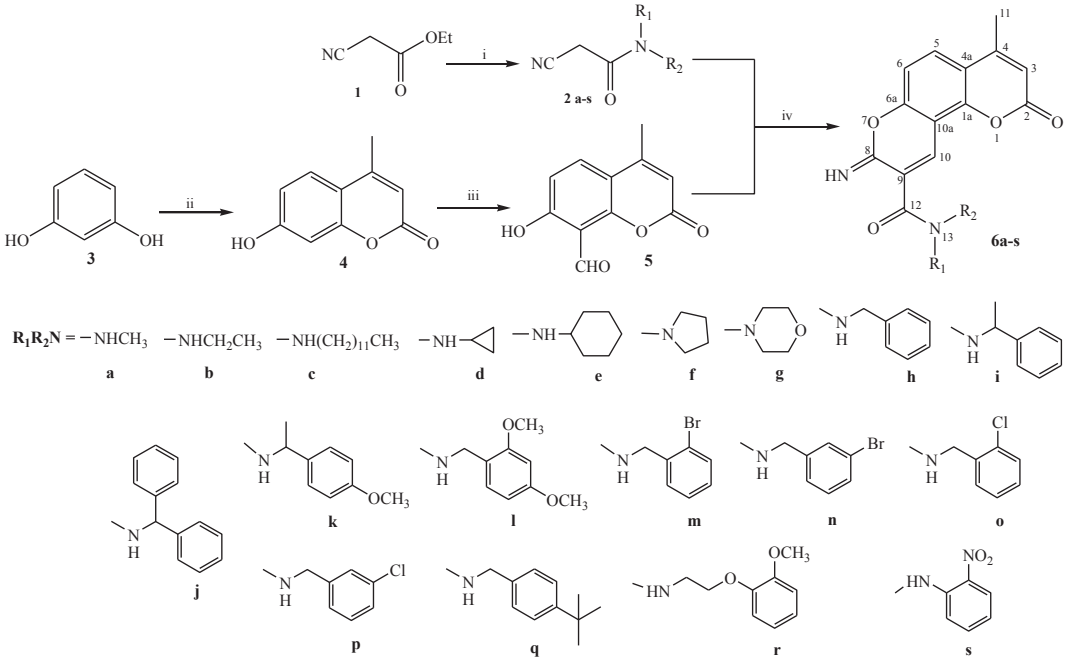


**Scheme 1.** Synthetic pathway of target compounds **6a-s**. *Reagents and conditions*: (i) corresponding amine, EtOH; (ii) ethylacetoacetate, $H_2SO_4$, 18 h; (iii) HMTA, glacial acetic acid, 90 °C, reflux, 6 h; (iv) $Et_3N$, EtOH.

[34], and compound **4** was treated with hexamethylenetetramine (HMTA) in glacial acetic acid, undergoes Duff formylation, to provide 8-formyl-7-hydroxy-4-methylcoumarin (**5**) [35]. Subsequently, compound **5** was condensed with different N-substituted cyano acetamide derivatives (**2a**–**s**) in the presence of $Et_3N$ afforded the final products (**6a**–**s**) [36]. An interesting feature of this procedure is the simple formation of final product without further purification. All the synthesized compounds were characterized by IR, $^1$H NMR, $^{13}$C NMR spectra and Mass spectrometry. In the IR spectrum, characteristic N–H absorption band of the imino group observed between 3415 and 3471 $cm^{-1}$, C=N characteristic absorption band between 1667 and 1689 $cm^{-1}$ and a singlet of the imino group proton resonated at 7.67–8.51 ppm in the $^1$H NMR spectrum further supported that –CHO, –OH and –CN groups involved in the reaction that leads to an extended iminopyran ring on coumarin moiety in the final product [36].

### 2.2. In vitro cholinesterase inhibition activity

To evaluate the potential application of fused tricyclic coumarins in the treatment of AD, the inhibition of AChE and BuChE activities was measured according to the spectrophotometric method of Ellman using galantamine, tacrine, donepezil and rivastigmine as positive control [37,38]. The $IC_{50}$ values and selectivity index for the inhibition of AChE and BuChE are summarized in Table 1. The target compounds showed different amounts of inhibitory activity to AChE with $IC_{50}$ values ranging from the submicromolar to micromolar range ($IC_{50}$ 0.003 ± 0.0007–2.6 ± 0.249 μM) and good inhibition selectivity (9.54–5793) against AChE over BuChE. Moreover, most of the synthetic derivatives exhibited AChE inhibitory activity ($IC_{50}$ 0.003 ± 0.0007–0.357 ± 0.027 μM) more potent than the positive control, galantamine, by 2–220 fold and their inhibition selectivity towards AChE increased about 194 fold compared with galantamine. Analogs **6c**, **6e** and **6m**–**q** showed stronger anti-AChE properties than all reference compounds. As far as BuChE is concerned, all analogs showed lesser inhibitory activity than galantamine, except compound **6b**, whereas all are less potent than donepezil, tacrine and rivastigmine. It was also demonstrated that **6n** displayed the most potent inhibitory activity on AChE with $IC_{50}$ value of 0.003 ± 0.0007 μM while **6b** was the most potent inhibitor of BuChE with $IC_{50}$ of 11.32 ± 1.38 μM. On the other hand, compounds **6b**, **6d** and **6r** could be considered as dual inhibitors of both enzymes.

From the data in Table 1 several conclusions can be drawn concerning the structure-activity relationships, and the effect of the substituents in phenyl ring of amide moiety. The change of the cyclopropyl moiety (**6d**) to cyclohexyl (**6e**) on amido part increased anti-AChE activity about 35 fold.

Meanwhile, elongation of aliphatic side chain in case of compounds **6a**, **6b** and **6c** increased the AChE inhibitory activity due to the more lipophilic property of these substituents. However, improvement in BuChE inhibitory activity was limited to N-ethyl group from N-methyl group. Replacement of the aliphatic methyl group (**6i**) at benzylic position by aromatic substituent (**6j**) led to an increase in the activity toward AChE but the BuChE inhibition activity was diminished. Interestingly, monosubstituted benzyl amide inhibitors **6m**–**6p** bearing electron withdrawing groups such as –Cl or –Br at *ortho* or *meta* positions were 110–700 fold more potent than inhibitor **6h** with simple benzyl moiety. Further, compound **6q** with *para*-(*ter*-butyl) benzyl moiety was also 210 folds more potent than compound **6h**. 2,4-Dimethoxy substitution at benzylamido moiety as in **6l** enhanced inhibition potency while 4-methoxy group on methyl benzylamido moiety (**6k**) diminished inhibition potency compared to the unsubstituted counterparts **6h** and **6i**, respectively.

### 2.3. In vitro antioxidant activity

The reduction of the oxidative stress is another crucial aspect in designing agents for AD treatment. We examined the antioxidant activities of our synthetic derivatives by using the ABTS (2,2′-azino-bis(3-ethylbenzthiazoline-6-sulfonic acid)) radical scavenging method [39]. Trolox, a water-soluble vitamin E analog, was used as a reference standard. The ability of compounds to scavenge radicals

**Table 1**
An *in vitro* AChE and BuChE inhibitory activities and ABTS radical scavenging capacity of synthetic fused tricyclic coumarin based compounds **6a**–**s** and reference compounds.

| Compounds | $IC_{50}$ (μM) ± S.E.M.[a] | | Selectivity for AChE[c] | $IC_{50}$ (μM) ± S.E.M.[a] |
|---|---|---|---|---|
| | AChE[b] | BuChE[b] | | ABTS radical scavenging activity |
| **6a** | 1.4 ± 0.087 | >100 | – | 34.16 ± 1.71 |
| **6b** | 0.294 ± 0.024 | 11.32 ± 1.38 | 38.5 | >50 |
| **6c** | 0.022 ± 0.0017 | >100 | – | >50 |
| **6d** | 0.91 ± 0.036 | 38.9 ± 2.83 | 42.74 | >50 |
| **6e** | 0.027 ± 0.004 | 42.05 ± 2.94 | 1557.4 | >50 |
| **6f** | 0.984 ± 0.008 | 73.08 ± 3.80 | 74.26 | >50 |
| **6g** | 0.115 ± 0.013 | NA | – | 11.27 ± 0.71 |
| **6h** | 2.13 ± 0.0517 | >100 | – | >50 |
| **6i** | 0.247 ± 0.019 | 35.84 ± 3.46 | 145.1 | 14.1 ± 1.10 |
| **6j** | 0.09 ± 0.005 | NA | – | >50 |
| **6k** | 1.9 ± 0.115 | NA | – | 9.04 ± 0.77 |
| **6l** | 0.357 ± 0.027 | >100 | – | >50 |
| **6m** | 0.016 ± 0.0021 | >100 | – | 11.94 ± 1.21 |
| **6n** | 0.003 ± 0.0007 | >100 | – | 7.98 ± 0.77 |
| **6o** | 0.012 ± 0.0018 | >100 | – | 15.99 ± 1.32 |
| **6p** | 0.019 ± 0.001 | >100 | – | 10.32 ± 0.84 |
| **6q** | 0.01 ± 0.0018 | 57.93 ± 1.81 | 5793 | 13.39 ± 0.25 |
| **6r** | 2.6 ± 0.249 | 24.8 ± 2.05 | 9.54 | 12.98 ± 1.07 |
| **6s** | 0.226 ± 0.0136 | >100 | – | >50 |
| Galantamine | 0.665 ± 0.02 | 19.78 ± 0.83 | 29.74 | – |
| Donepezil | 0.038 ± 0.002 | 7.69 ± 0.42 | 202.36 | – |
| Tacrine | 0.372 ± 0.14 | 1.77 ± 0.13 | 4.75 | – |
| Rivastigmine | 3.4 ± 0.83 | 5.5 ± 1.3 | 1.61 | – |
| Trolox | – | – | – | 27.35 ± 1.34 |

[a] Concentration required to produce 50% inhibition of enzyme activity. $IC_{50}$ values are given as the mean of three independent determinations.
[b] AChE from Electric Eel and BuChE from equine serum were used.
[c] Selectivity ratio = ($IC_{50}$ of BuChE)/($IC_{50}$ of AChE).

was shown as $IC_{50}$, the test compound's concentration resulting in 50% inhibition of free radical (Table 1). According to the data, ten synthetic derivatives were found to possess potent ABTS radical scavenging capacities with $IC_{50}$ values in the range of 7.98–34.16 μM. Among all nineteen synthetic analogs, nine compounds showed higher radical scavenging activities ($IC_{50}$ range of 7.98–15.99 μM) than trolox ($IC_{50}$ of 27.35 μM) which is 1.7–3.4 fold of trolox. The best results were obtained with derivatives bearing 3-bromo or 4-methoxy group on phenyl ring of benzyl amido moiety. Compound **6g** with heterocyclic amide moiety displayed higher radical scavenging property than their alicyclic counterparts. Converting methyl to benzyl as in **6a** to **6n** diminishes the antioxidant activity. Introduction of methoxy group on 4-position of phenyl ethyl amido moiety as in **6k** enhances the radical scavenging activity by 1.5 fold. The radical scavenging capacity of compounds increased from *ortho* to *meta* halo substitution as can be seen in **6m**–**6p**.

### 2.4. Neurotoxicity of compounds in SK N SH cells

To investigate the effect of the selected compounds (**6m**, **6n**, **6o**, **6p** and **6q**) and galantamine as reference on cell viability, the MTT (3-(4,5-dimethylthiazol-2-yl)-2,5-diphenyltetrazolium bromide) assay was conducted on SK N SH cells (human neuroblastoma cell line) [40,41]. The SK N SH cells were incubated with varying concentrations (40, 80, 120, 160 and 200 μM) of the test compounds and galantamine for 24 h and measured cell viability. The results depicted in Fig. 1 revealed that under these conditions all of the tested compounds were nontoxic to SK N SH cells at any of the concentrations tested except **6n** and **6q**.

### 2.5. Neuroprotective effect against $H_2O_2$-induced cell death in SK N SH cells

The neuroprotective capacities of selected compounds (**6m**–**q**) against oxidative stress were evaluated by assessing the ability of the tested compounds to protect against $H_2O_2$-induced SK N SH cell injury using the MTT assay [40,41]. As estimated by MTT assay, cell viability is markedly decreased to 60% after 1.0 mM $H_2O_2$ exposure for 24 h. However, when cells were preincubated with compounds (40, 80, 120 μM) for 3 h, and then exposed to $H_2O_2$, cell toxicity was significantly attenuated in a dose-dependent manner and also brought to control levels at higher concentrations (Fig. 2). Addition of compound to the medium prior to $H_2O_2$ addition increases survival cells by preventing $H_2O_2$ induced oxidative stress caused cell death indicating that these compounds act as a potential oxidative suppressors. Catechin was included as a reference antioxidant compound.

### 2.6. Kinetic study of the AChE inhibition

To gain further insight into the mechanism of action on AChE of this family of compounds, a kinetic study was carried out on compound **6n**, the most potent AChE inhibitor. For this purpose, the rate of the enzyme activity was measured at three different concentrations of compound **6n** using different concentrations of the substrate acetylthiocholine iodide (ATCh). In each case, the initial velocity was measured at different concentrations of the substrate (S), and the reciprocal of the initial velocity (1/v) was plotted against the reciprocal of [ATCh].

Graphical analysis of the reciprocal Lineweaver Burk plots (Fig. 3) showed both increased slopes and intercepts at increasing concentration of the inhibitor and intersection of double reciprocal lines in the upper left quadrant. This pattern indicates a mixed-type inhibition [42]. Generally, this type of inhibition suggests binding to free enzyme and enzyme–substrate complex. Thus, this result indicated that compound **6n** was able to bind at both the catalytic and peripheral site of AChE. The inhibitory constants ($K_{i1}$ and $K_{i2}$) for the compound **6n** were calculated as 0.0103 μM (binding to free enzyme) and 0.0193 μM (binding to enzyme–substrate complex)

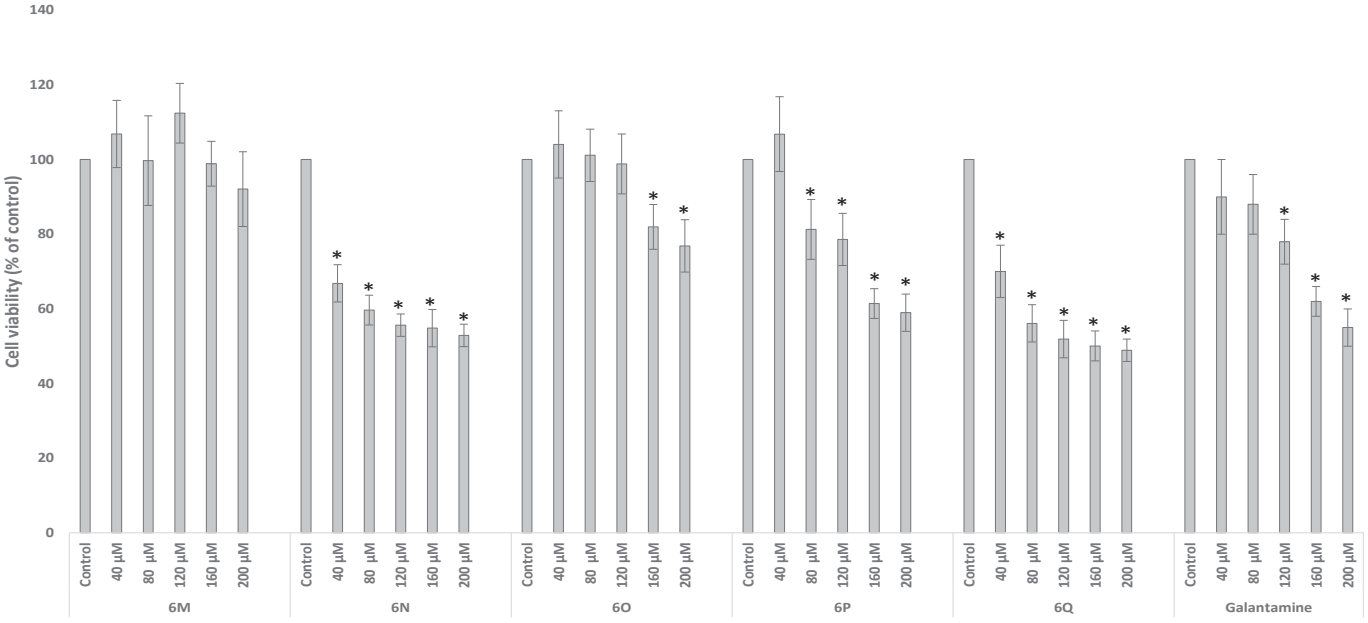


**Fig. 1.** Neurotoxic effects of **6m**, **6n**, **6o**, **6p** and **6q** on SK N SH cells (human neuroblastoma cell line). Bar chart show the percentage of cell viability in the presence or absence (control) of indicated concentrations of **6m**, **6n**, **6o**, **6p**, **6q**, and Galantamine. MTT assay was done to assess cell viability. Cell viability corresponding to control cells was considered as 100%. The values represent the mean SEM of three independent experiments, each one performed by triplicate in different cell batches. Statistics show neurotoxic effects of these compounds versus controls. *P < 0.05 versus 100% cell viability (one-way ANOVA test).

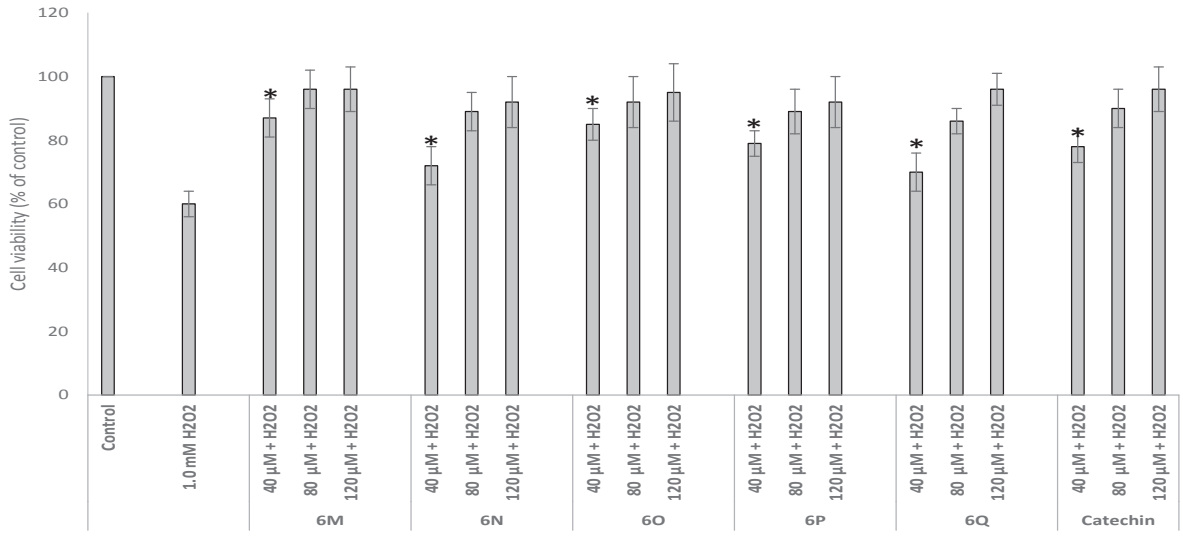


**Fig. 2.** Neuroprotective activity of compounds **6m**, **6n**, **6o**, **6p**, **6q** and catechin against $H_2O_2$ induced cell death in SK N SH cells. Cells were treated with different concentrations 40 μM–120 μM of the compound for 3 h. After 24 h, cell viability was determined by MTT assay in the presence of 1.0 mM $H_2O_2$. The values represent the mean SEM of three independent experiments, each one performed by triplicate in different cell batches. Statistics show neurotoxic effects of these compounds versus controls. *P < 0.05 versus $H_2O_2$ treatment.

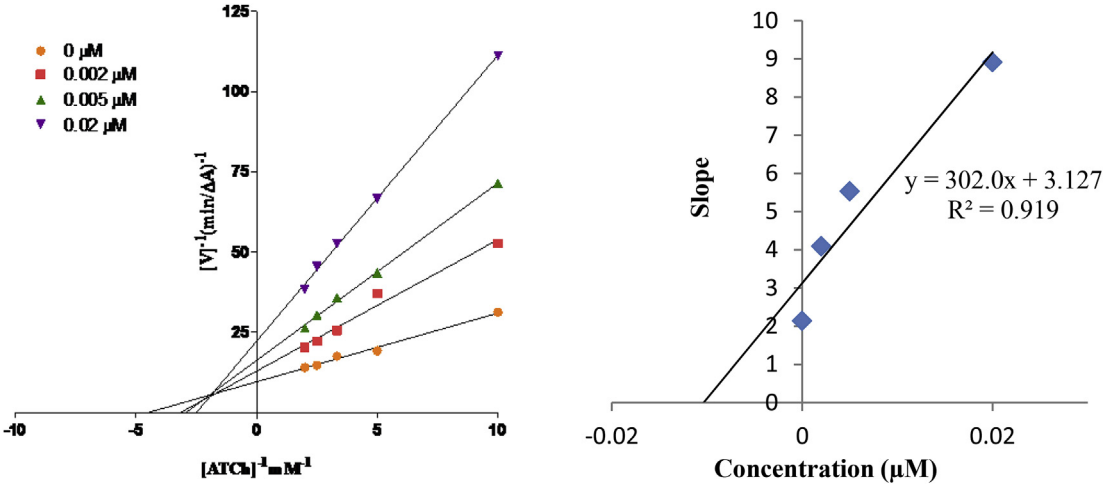


**Fig. 3.** Steady-state inhibition of AChE by compound **6n**. (Left) Lineweaver Burk plot of reciprocal of initial velocities versus reciprocal of acetylthiocholine iodide concentrations (0.1–0.5 mM) in the absence and presence of **6n** at 0.002 μM, 0.005 μM and 0.02 μM; (right) secondary plots of the Lineweaver Burk plot, slope versus various concentrations of **6n**.

using secondary plots.

### 2.7. Molecular modeling study

A molecular modeling study was performed to investigate possible binding mode of fused tricyclic coumarin derivatives to the cholinesterase enzymes utilizing a docking program, Schrödinger maestro software (version 9.2; Schrödinger LLC, NewYork). For this purpose, five most potent compounds (**6m**–**q**) with $IC_{50}$ values below 0.02 μM were docked into the active site of the *Ee*AChE. The 3D structure of *Ee*AChE (from Electric eel) was retrieved from PDB (PDB ID: 1C2O) [43]. The results were characterized by the G Scores obtained from GLIDE (Grid-based Ligand Docking with Energetics) docking [44]. The best docked poses in terms of the Glide energy of binding were further analyzed to clarify interactions between target compounds and AChE. Exhaustive analysis of the docking poses showed that compounds **6m, 6o** and **6q** were similarly oriented in the active site. However, the binding modes of **6n** and **6p** were significantly different from the binding modes of **6m, 6o** and **6q** at the AChE active site gorge. The binding poses within AChE along with the residues surrounding derivatives **6m, 6o** and **6q** are depicted in Fig. 4.

As can be seen in Fig. 4, the docking orientation of **6m, 6o** and **6q** places the ligand in the PAS with the fused tricyclic coumarin moiety sandwiched between Trp 286 (4.7 Å) and Tyr 341 (4.5 Å) residues by π–π stacking. The 2-bromo benzylamido moiety extended to the opening of the PAS and forms CH … π interaction with side chain of Glu 292 (4.0 Å). In this orientation, the coumarin carbonyl group establishes hydrogen bond interaction with the hydroxyl group of Phe 295. Also compounds **6m, 6o** and **6q** were all able to protrude out of the AChE gorge, a feature which is considered important for the AChE-induced Aβ aggregation inhibition.

The orientation of ligands **6n** and **6p** is reversed comparing to the pose of **6m, 6o** and **6q**. As shown in Fig. 4, the ligand was well accommodated in the gorge of AChE active site so that the benzylamido moiety was leaning toward the CAS. Specifically, 3-halo phenyl ring of benzylamido moiety stacks against the Phe 338 via T-shape (edge-to-face) π–π interaction and potentially induce

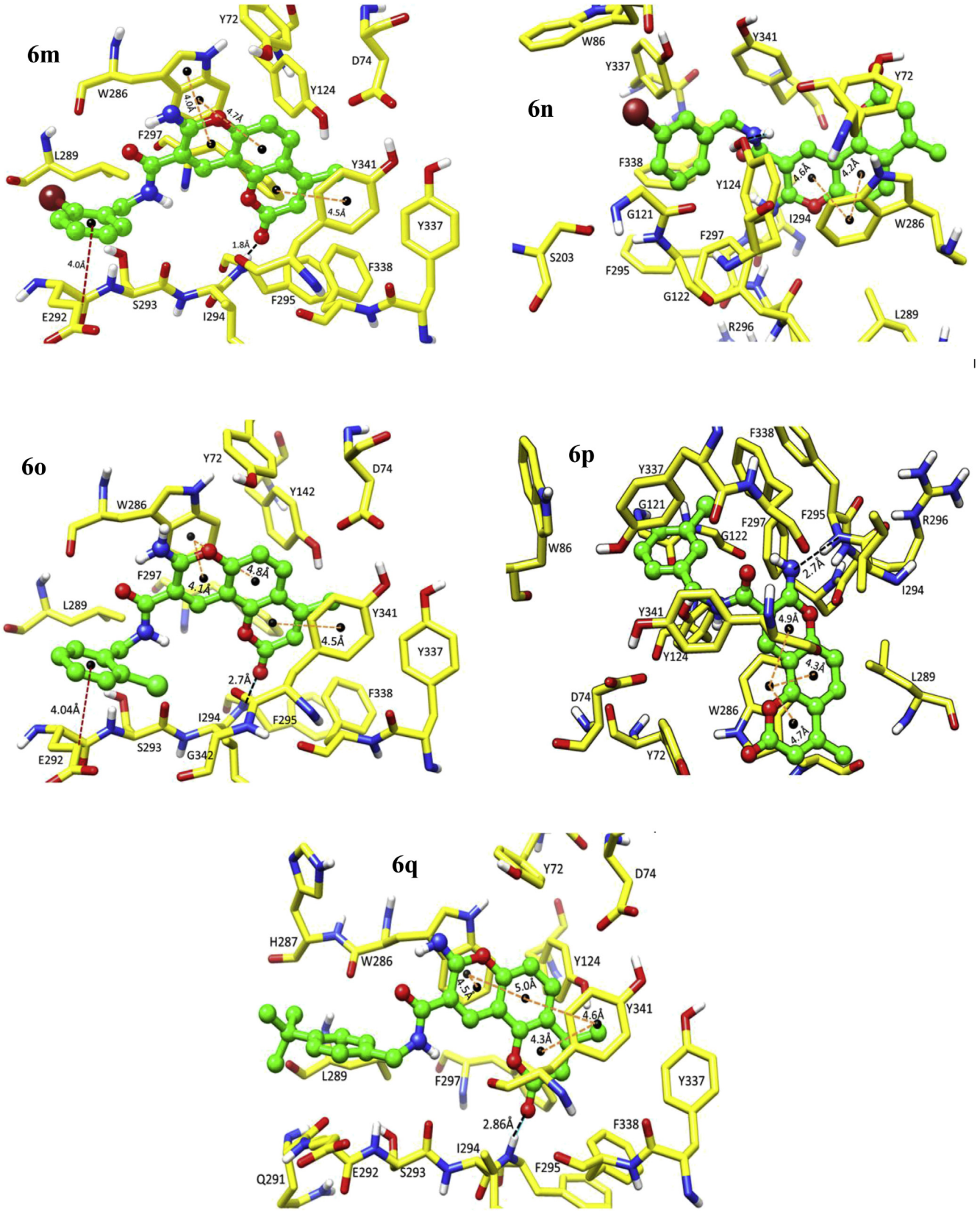


**Fig. 4.** Docking pose of the test compounds **6m**–**q** at the binding site of AChE predicted by molecular modeling.

hydrophobic interactions with residues Tyr 337, Trp 86, Phe 295, Gly 121 and Ser 203. However, no interactions with the catalytic triad residues have been found. In this binding mode, the tricyclic coumarin scaffold formed π-stacking with aromatic ring of indole moiety of Trp 286 in the PAS. The coumarin carbonyl group in **6n** was hydrogen-bonded to Tyr 72. In addition, amide –NH group

establishes hydrogen bond interaction with –OH group of Tyr 124 in the mid gorge site. This binding mode is in agreement with mixed-mode inhibition pattern of **6n**, in which both CAS and PAS are occupied by the ligand. However, instead **6p** disclosed only one hydrogen bonding interactions between imino –NH and Phe 295.

With respect to BuChE, in the absence of X-ray structure of *Eq*BuChE (from Horse serum), a 3D structure was predicted by homology modeling approach [43]. The template considered for homology modeling of BuChE yielded 2PM8 as the suitable structural template with 94% query coverage and 90% sequence similarity. To explore possible binding modes for the most active compounds **6b** and **6r** toward BuChE, they were docked into BuChE active site. The best ranked docking results revealed that BuChE can effectively accommodate the compounds **6b** and **6r** inside the active site gorge (Fig. 5). The aromatic amino acid residues like Tyr 72, Tyr 124, Trp 286, Phe 295, Phe 297 and Tyr 337 in AChE are mostly replaced by aliphatic ones: Asn 68, Gln 119, Ala 277, Leu 286, Val 288, and Ala 328 in BuChE. This variation might have faded the ability of BuChE to form π–π stacking interactions compared to AChE. The **6r**–BuChE complex was found to be stabilized mainly by the hydrophobic interactions with all the active site residues existing along the wall of the active site gorge which includes PAS, Anionic subsite, Oxyaninon hole, catalytic triad, and choline binding region of the enzyme. The 2-(2-methoxyphenoxy)ethyl amide moiety of **6r** found to be protruding into the space between the residues Trp 110 and Ala 356 of anionic subsite and forming hydrophobic interactions with residues Ala 356, Phe 357, Trp 458, and Met 465. In the complex, Trp 110 was found to allow for further π–π stacking interactions with the iminopyran ring of the ligand. The oxygen atom of the phenoxy is also forming a hydrogen bond with His 466 of the catalytic triad.

The binding mode of compound **6b**, shown in Fig. 5, places the ligand within the central region of the active site gorge where substrate or inhibitors reported to bind effectively. In this orientation, Phe 357 allowed a π–π stacking interaction with the tricyclic coumarin moiety at choline binding site of the BuChE. Ligand **6b** exhibited two strong hydrogen bond interactions with amino acids of the catalytic triad, they are between oxygen of coumarin moiety and –OH group of Ser 226 and between amide carbonyl and –NH group of His 466. The N-ethyl group on the amide part forms CH … .π interaction with Trp 110. In addition **6b** interact with Trp110, Leu 313, Leu 314, Val 316, Ala 356, Ile 426, Trp 458, Met 465, and Tyr 468 residues via hydrophobic interactions. Conversely to the **6r**-BuChE complex, the favorable position of **6b** within the gorge accounts for a higher affinity of **6b** towards BuChE and makes it a more potent BuChE inhibitor than compound **6r**.

### 2.8. Theoretical ADMET analysis of fused coumarins

Finally, a series of theoretical calculations using QikProp (Version 3.5, Schrödinger, LLC, New York, NY, 2012) and $LC_{50}$ values (Lethal concentration 50%) using http://lazar.in-silico.de/predict allowed us to predict the ADMET (Absorption, Distribution, Metabolism, Excretion and Toxicity) properties of target compounds (**6a**–**s**) within the organism [31,45]. The four criterion ADME influence the drug levels, its kinetics and exposure to the tissues, and hence the performance and pharmacological activity of a drug. About 45 physically significant descriptors and pharmacologically relevant properties of these compounds were predicted and some of the important properties were analyzed (Table S1, Supplementary Material). Based on the predicted values for BBB penetration, all compounds might be able to penetrate into the CNS and therefore, are considered as active compounds on the CNS. CNS drugs show values of MW < 450, HB donor <3, HB acceptors <10, QPlogPo/w < 6, TPSA < 140, number of rotatable bonds <8 and hydrogen bonds <8 CNS, in a smaller range than general therapeutics [46,47]. All the active compounds satisfied the characteristics of CNS acting drugs as all predicted values are in the limits. The solubility (QPlogS) of organic molecules in water has a significant impact on many ADME-related properties like uptake, distribution, transport, and eventually bioavailability. All compounds showed solubility values within the limits [48]. Moreover, all the compounds may not show either acute toxicity according to the calculated $LC_{50}$ values nor mutagenic effect with respect to the AMES test data. In addition, the Lipinski criteria for the target compounds were predicted. According to Lipinski criteria of drug likeness, all the compounds (**6a**–**6s**) within the range set by Lipinski's rule of five and could be good candidate for drug development.

### 2.9. Determination of brain AChE activity

Anti-Alzheimer drug candidate, like any other CNS drug, must be able to efficiently enter into the brain, for which a major

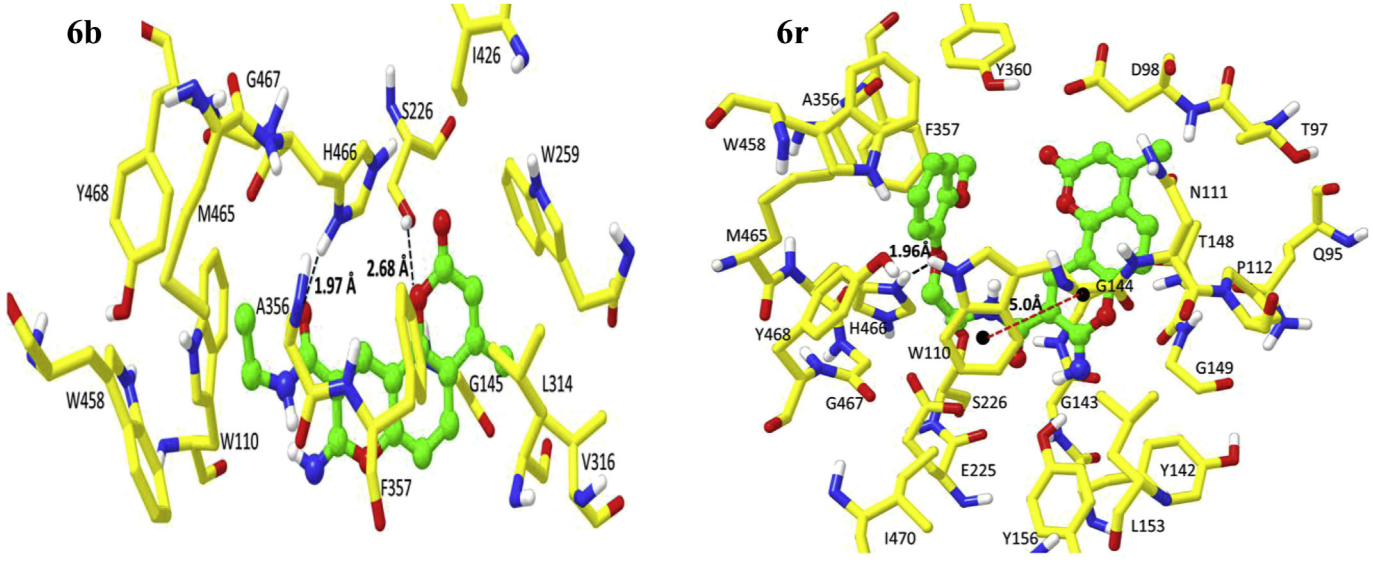


**Fig. 5.** Docking pose of the test compounds **6b** and **6r** at the binding site of BuChE predicted by molecular modeling.

requirement is to cross the blood brain barrier (BBB). Thus, to determine whether the compound **6n** could penetrate the BBB, the brain AChE activity was measured as an indirect method [49]. Different concentrations of most active compound **6n** (16, 50, 100 and 200 mg/kg) was administered via intraperitoneal injection to male mice (30 ± 2 g). After 48 h of administration, mice were sacrificed and brain homogenates were prepared. Supernatant of brain homogenate was used to determine brain AChE activity. The rate of hydrolysis of ATCh (15 μL of 1 mM) by brain AChE at 10, 20, 30, 40 and 50 μL was measured using Ellman method. As presented in Fig. 6, the rate of hydrolysis of ATCh by brain AChE was decrease with increase in administratered dose of **6n**. Therefore, after treatment with **6n**, the brain AChE activity was found to be down regulated in dose dependent manner which is possible only if **6n** had penetrated the blood–brain barrier and inhibit brain AChE activity.

## 3. Conclusion

In summary, nineteen new iminopyran fused tricyclic coumarin derivatives were synthesized and evaluated as novel multifunctional agents against AD with selective, dual binding site AChE inhibitory and antioxidant activities. The biological evaluation showed that most of these molecules were potent and selective AChE inhibitors, which is 2–220 folds more potent than the positive control, galantamine. Especially **6n** bearing 2-bromobenzyl amide moiety was found to be most potent AChE inhibitor ($IC_{50}$ 0.003 ± 0.0007 μM) with strong ABTS radical scavenging activity (7.98 ± 0.77 μM). Compound **6b** exhibited the highest BuChE inhibition potency. Besides, compound **6q** with *ter*-butyl group on *para* position of benzyl amido moiety was the highest selective AChE inhibitor (SI 5793). It is worth highlighting that all assayed compounds exhibiting not only no neurotoxicity but even a strong neuroprotective effect than catechin, reference compound. Both the inhibition kinetic and docking studies demonstrated the capability of prototype compounds to bind with the CAS and PAS of AChE simultaneously, and inducing a strong inhibitory effect. *In silico* ADMET prediction indicated that compounds are CNS active and comply with the Lipinski's rule of five. An *in vivo* brain AChE activity study indicated that **6n** would probably cross the Blood Brain Barrier. Altogether, the results suggest that the tricyclic fused coumarin derivatives, in particular compound **6n**, can be considered as potential therapeutic agents for AD. The work also presents a new family of multifunctional leading structures for developing novel anti-AD drugs.

## 4. Experimental section

### 4.1. General information

All commercially available starting materials and reagents were purchased from Merck and were used without further purification. Reaction progress was monitored using analytical thin layer chromatography (TLC) on precoated silica gel 60 $F_{254}$ aluminum plates and the spots were detected under UV light (254 nm). Melting points were measured on GUNA melting point apparatus and were uncorrected. The IR spectra were taken as KBr discs using Perkin Elmer Spectrum 2 spectrophotometer (Singapore). The NMR spectra were recorded on a Bruker spectrometer operating at 400 MHz ($^1$H) and at 100 MHz ($^{13}$C). The chemical shifts (δ) and coupling constants (*J*) are expressed in parts per million and hertz, respectively. Splitting patterns are designated as s, singlet; d, doublet; t, triplet; m, multiplet. The atoms numbering of the intermediate and target compounds used for NMR data are depicted in Scheme 1. Mass spectra were determined on an Agilent LC/MSD trap SL 1100 series spectrometer with a 70 eV (ESI probe) and high-resolution mass spectra were obtained by using ESI-QTOF mass spectrometry.

### 4.2. General procedure for the synthesis of N-substituted cyano acetamide derivatives (*2a–s*)

To a solution of different amines (1 mmol) in ethanol (10 mL), ethylcyanoacetate (1.2 mmol) was added. The reaction mixture was stirred for 5–8 h under reflux. Progress of the reaction was monitored by TLC. After completion of the reaction, the resulting mixture was cooled to 0–5 °C in an ice bath and the solid separated was filtered off [32,33].

### 4.3. Representative procedure for the preparation of 7-hydroxy-4-methylcoumarin (*4*)

In a round bottom flask (100 mL), charged conc. sulfuric acid (20.00 mL) and cooled to 0–5 °C in an ice bath. A solution of resorcinol (1 mmol) in ethylacetoacetate (1.5 mmol) was added to sulfuric acid under constant stirring at 0–5 °C. The reaction mixture was stirred overnight at room temperature, then it was slowly poured into crushed ice and the resulting solid was separated by filtration and washed successively with water. The product was dried and recrystallized with ethanol to get compound **4** [34].

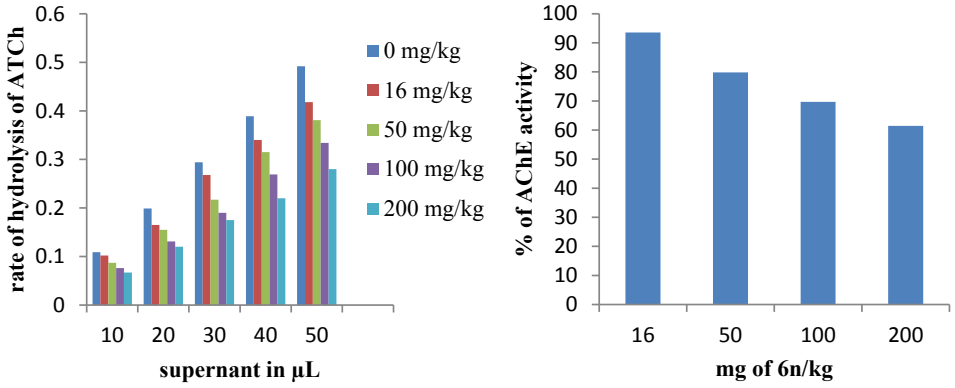


**Fig. 6.** Determination of brain AChE activity to assess BBB penetration of **6n**. (left) Rate of hydrolysis of ATCh by AChE in brain homogenates from mice injected with **6n**; (right) AChE activity of brain homogenates from mice injected with **6n**, expressed as a percentage of the AChE activity of corresponding preparations from control mice.

### 4.4. Synthetic procedure for 8-formyl-7-hydroxy-4-methylcoumarin (**5**)

A reaction mixture of **4** (20 g, 114 mmol) and hexamethylenetetramine (40 g, 285 mmol) in glacial acetic acid (150 mL) was stirred for 5.5 h at 95 °C. Thereafter, aqueous solution of HCl (300 mL, conc. $HCl/H_2O$ = 84:100, v/v) was added, stirred further for 0.5 h at 70 °C and then the final reaction mixture after cooling was poured into ice water. The resulting solution was exhaustively extracted with ethyl acetate. The combined organic extracts were dried over $Na_2SO_4$ and the solvent was removed under reduced pressure. The crude solid was purified by crystallization from ethylacetate [35].

### 4.5. General synthetic procedure for synthesis of final product: (**6a**–**s**)

To a solution of **5** (1.5 mmol) and **2a**–**s** (3.1 mmol) in ethanol (10 mL) was added $Et_3N$ (0.1 mmol) drop wise at room temperature. The resulting mixture was stirred at 50 °C for 2–3 h and then allowed to cool to room temperature. The product was precipitated from the reaction mixture, collected by filtration and washed with methanol (2–3 mL) to yield corresponding final products (**6a**–**s**) [36].

#### 4.5.1. N9,4-dimethyl-8-imino-2-oxo-2H,8H-pyrano[2,3-f]chromene-9-carboxamide (**6a**)

Off white solid; yield 69%; mp: 150–152 °C; IR (KBr) $\nu_{max}$: 3415, 3309 (N–H), 2986, 2927, 1738 (C=O), 1685 (C=N), 1631 (C=O), 1528, 1386, 1284, 1068, 862, 817, 579 $cm^{-1}$; $^1H$ NMR (400 MHz, DMSO-$d_6$) δ: 9.99 (br s, 1H, 13-NH), 9.29 (s, 1H, 10-H), 8.51 (s, 1H, 8-NH), 7.88 (d, 1H, $J$ = 8.4 Hz, 5-H), 7.16 (d, 1H, $J$ = 8.4 Hz, 6-H), 6.40 (s, 1H, 3-H), 2.85 (br s, 3H, 1′-$CH_3$), 2.43 (s, 3H, 11-$CH_3$); $^{13}C$ NMR (100 MHz, DMSO-$d_6$) δ: 167.9 (C-2), 164.9 (C-8), 161.8 (C-12), 159.7 (C-1a), 153.3 (C-4), 152.5 (C-6a), 151.3 (C-10), 125.4 (C-5), 116.6 (C-4a), 115.6 (C-9), 113.7 (C-3), 112.9 (C-10a), 109.3 (C-6), 32.4 (C-1′), 19.0 (C-11); ESI-MS *m/z*: 286.1 $[M+H]^+$; HRMS calcd. for $C_{15}H_{13}O_4N_2$: 285.0876, found: 285.0885.

#### 4.5.2. N9-ethyl-8-imino-4-methyl-2-oxo-2H,8H-pyrano[2,3-f]chromene-9-carboxamide (**6b**)

Reddish brown solid; yield 70%; mp: 151–154 °C; IR (KBr) $\nu_{max}$: 3443, 3250 (N–H), 3079, 2853, 2854, 2926, 1733 (C=O), 1671 (C=N), 1627 (C=O), 1552, 1445, 1387, 1191, 1072, 847, 772, 585 $cm^{-1}$; $^1H$ NMR (400 MHz, $CDCl_3$) δ: 9.97 (br s, 1H, 13-NH), 8.93 (s, 1H, 10-H), 7.71 (s, 1H, 8-NH), 7.63 (d, 1H, $J$ = 8.8 Hz, 5-H), 7.03 (d, 1H, $J$ = 8.8 Hz, 6-H), 6.24 (s, 1H, 3-H), 3.46 (m, 2H, 1′-$CH_2$), 2.42 (s, 3H, 11-$CH_3$), 1.23 (t, 3H, $J$ = 13.2 Hz, 2′-$CH_3$); $^{13}C$ NMR (100 MHz, $CDCl_3$) δ: 161.3 (C-2), 159.2 (C-8), 156.4 (C-12), 155.4 (C-1a), 152.0 (C-4), 150.9 (C-6a), 134.6 (C-10), 127.9 (C-5), 121.3 (C-4a), 115.8 (C-9), 114.0 (C-3), 111.5 (C-10a), 108.6 (C-6), 34.8 (C-1′), 18.9 (C-11), 14.7 (C-2′); ESI-MS *m/z*: 299.1 $[M+H]^+$; HRMS calcd. for $C_{16}H_{15}O_4N_2$: 299.10263, found: 299.10267.

#### 4.5.3. N-dodecyl-8-imino-4-methyl-2-oxo-2H,8H-pyrano[2,3-f]chromene-9-carboxamide (**6c**)

Orange solid; yield 50%; mp: 164–167 °C; IR (KBr) $\nu_{max}$: 3440, 3321 (N–H), 3204, 3067, 2956, 2921, 2852, 1726 (C=O), 1679 (C=N), 1642, 1625 (C=O), 1584, 1201, 1080, 858, 771 $cm^{-1}$; $^1H$ NMR (400 MHz, $CDCl_3$) δ: 10.00 (br s, 1H, 13-NH), 8.89 (s, 1H, 10-H), 7.71 (s, 1H, 8-NH), 7.63 (d, 1H, $J$ = 8.8 Hz, 5-H), 7.02 (d, 1H, $J$ = 8.8 Hz, 6-H), 6.22 (s, 1H, 3-H), 3.41 (q, 2H, $J$ = 6 Hz, 1′-$CH_2$), 2.41 (s, 3H, 11-$CH_3$), 1.58 (m, 2H, 2′- $CH_2$), 1.24 (br s, 18H, 3′–11′- $CH_2$) 0.86 (t, 3H, $J$ = 6.8 Hz, 12′-$CH_3$); $^{13}C$ NMR (100 MHz, $CDCl_3$) δ: 161.3 (C-2), 159.2 (C-8), 156.4 (C-12), 155.4 (C-1a), 152.0 (C-4), 150.8 (C-6a), 134.4 (C-10), 127.9 (C-5), 121.3 (C-4a), 115.8 (C-9), 114.0 (C-3), 111.5 (C-10a), 108.5 (C-6), 40.0 (C-1′), 32.0 (C-2′), 29.7 (C-3′), 29.7 (C-4′), 29.7 (C-5′), 29.6 (C-6′), 29.4 (C-7′), 29.4 (C-8′,9′), 27.2 (C-10′), 22.8 (C-11′), 18.9 (C-11), 14.2 (C-12′); ESI-MS *m/z*: 439.4 $[M+H]^+$; HRMS calcd. for $C_{26}H_{35}O_4N_2$: 439.2598, found: 439.2604.

#### 4.5.4. N9-cyclopropyl-8-imino-4-methyl-2-oxo-2H,8H-pyrano[2,3-f]chromene-9-carboxamide (**6d**)

Yellow solid; yield 70%; mp: 115–117 °C; IR (KBr) $\nu_{max}$: 3447, 3289 (N–H), 3063, 2950, 2876, 1739 (C=O), 1675 (C=N), 1625 (C=O), 1574, 1452, 1386, 1346, 1203, 1195, 820, 767, 598 $cm^{-1}$; $^1H$ NMR (400 MHz, $CDCl_3$) δ: 10.05 (d, 1H, $J$ = 2.4 Hz, 13-NH), 8.92 (s, 1H, 10-H), 7.67 (s, 1H, 8-NH), 7.64 (d, 1H, $J$ = 8.8 Hz, 5-H), 7.02 (d, 1H, $J$ = 8.8 Hz, 6-H), 6.24 (s, 1H, 3-H), 2.97–2.94 (m, 1H, 1′-H), 2.42 (s, 3H, 11-$CH_3$), 0.86–0.59 (m, 4H, 2′- $CH_2$, 3′- $CH_2$); $^{13}C$ NMR (100 MHz, $CDCl_3$) δ: 162.8 (C-2), 159.2 (C-8), 156.4 (C-12), 155.4 (C-1a), 152.1 (C-4), 150.9 (C-6a), 134.5 (C-10), 128.0 (C-5), 121.0 (C-4a), 115.8 (C-9), 114.0 (C-3), 111.5 (C-10a), 108.5 (C-6), 23.0 (C-1′), 18.9 (C-11), 6.65 (C-2′, C-3′); ESI-MS *m/z*: 311.1 $[M+H]^+$; HRMS calcd. for $C_{17}H_{15}O_4N_2$: 311.1032, found: 311.1036.

#### 4.5.5. N9-cyclohexyl-8-imino-4-methyl-2-oxo-2H,8H-pyrano[2,3-f]chromene-9-carboxamide (**6e**)

Orange solid; yield 71%; mp: 148–151 °C; IR (KBr) $\nu_{max}$: 3461, 3285 (N–H), 3190, 2924, 1737 (C=O), 1675 (C=N), 1626 (C=O), 1578, 1447, 1391, 1347, 1279, 1172, 821, 770 $cm^{-1}$; $^1H$ NMR (400 MHz, $CDCl_3$) δ: 10.02 (d, 1H, $J$ = 7.2 Hz, 13-NH), 8.90 (s, 1H, 10-H), 7.71 (s, 1H, 8-NH), 7.63 (d, 1H, $J$ = 8.8 Hz, 5-H), 7.02 (d, 1H, $J$ = 8.8 Hz, 6-H), 6.23 (s, 1H, 3-H), 3.97 (m, 1H, 1′-H), 2.42 (s, 3H, 11-$CH_3$), 1.96 (m, 4H, 2′- $CH_2$, 6′-$CH_2$), 1.24 (m, 6H, 3′–5′-$CH_2$); $^{13}C$ NMR (100 MHz, $CDCl_3$) δ: 160.3 (C-2), 159.2 (C-8), 156.4 (C-12), 155.4 (C-1a), 152.1 (C-4), 150.8 (C-6a), 134.5 (C-10), 127.8 (C-5), 121.5 (C-4a), 115.7 (C-9), 114.0 (C-3), 111.5 (C-10a), 108.6 (C-6), 48.4 (C-1′), 32.7 (C-2′,5′), 25.8 (C-4′), 24.6 (C-3′,5′), 18.9 (C-11); ESI-MS *m/z*: 353.1 $[M+H]^+$; HRMS calcd. for $C_{20}H_{21}O_4N_2$: 353.1502, found: 353.1510.

#### 4.5.6. 8-imino-4-methyl-9-(tetrahydro-1H-1-pyrrolylcarbonyl)-2H,8H-pyrano[2,3-f]chromen- 2-one (**6f**)

Pale reddish brown solid; yield 63%; mp: 140–144 °C; IR (KBr) $\nu_{max}$: 3439, 3057, 2956, 2924, 2855, 1732 (C=O), 1686 (C=N), 1627 (C=O), 1591, 1575, 1449, 1388, 1169, 1085, 834, 592 $cm^{-1}$; $^1H$ NMR (400 MHz, $CDCl_3$) δ: 8.49 (s, 1H, 10-H), 7.82 (s, 1H, 8-NH), 7.77 (d, 1H, $J$ = 8.8 Hz, 5-H), 7.10 (d, 1H, $J$ = 8.8 Hz, 6-H), 6.31 (s, 1H, 3-H), 3.63 (m, 2H, 2′-$CH_2$), 3.44 (m, 2H, 5′-$CH_2$), 2.47 (s, 3H, 11-$CH_3$), 1.95 (m, 4H, 3′- $CH_2$, 4′- $CH_2$); $^{13}C$ NMR (100 MHz, $CDCl_3$) δ: 162.6 (C-2), 158.8 (C-8) 156.9 (C-12), 155.8 (C-1a), 152.3 (C-4), 150.4 (C-6a), 136.1 (C-10), 128.2 (C-5), 126.4 (C-4a), 116.1 (C-9), 114.4 (C-3), 112.8 (C-10a), 108.1 (C-6), 47.8 (C-2′), 46.3 (C-5′), 26.0 (C-3′), 24.4 (C-4′), 19.0 (C-11); ESI-MS *m/z*: 326.1 $[M+H]^+$; HRMS calcd. for $C_{18}H_{17}O_4N_2$: 326.10278, found: 326.10268.

#### 4.5.7. 8-imino-4-methyl-9-(morpholinocarbonyl)-2H,8H-pyrano[2,3-f]chromen-2-one (**6g**)

Pale yellow solid; yield 58%; mp: 137–140 °C; IR (KBr) $\nu_{max}$: 3436, 3073, 2924, 2853, 1727 (C=O), 1667 (C=N), 1637 (C=O), 1593, 1573, 1466, 1373, 1275, 1201, 1108, 1067, 847, 770, 593 $cm^{-1}$; $^1H$ NMR (400 MHz, $CDCl_3$) δ: 8.50 (s, 1H, 10-H), 7.82 (s, 1H, 8-NH), 7.60 (d, 1H, $J$ = 8.8 Hz, 5-H), 7.03 (d, 1H, $J$ = 8.8 Hz, 6-H), 6.25 (s, 1H, 3-H), 3.77 (t, 4H, 3′-$CH_2$, 5′-$CH_2$), 3.58 (t, 4H, 2′-$CH_2$, 6′-$CH_2$), 2.43 (s, 3H, 11-$CH_3$); $^{13}C$ NMR (100 MHz, $CDCl_3$) δ: 164.3 (C-2,8), 159.5 (C-12), 155.4 (C-1a), 152.4 (C-4), 150.1 (C-6a), 137.0 (C-10), 127.5 (C-5), 121.5 (C-4a), 115.7 (C-9), 113.8 (C-3), 111.9 (C-10a), 107.6 (C-6), 66.8 (C-3′,5′), 47.4 (C-2′,6′), 18.9 (C-11); ESI-MS *m/z*: 341.1 $[M+H]^+$; HRMS calcd. for $C_{18}H_{17}O_5N_2$: 341.11320, found: 341.11347.

*4.5.8. N9-benzyl-8-imino-4-methyl-2-oxo-2H,8H-pyrano[2,3-f] chromene-9-carboxamide (**6h**)*

Pale yellow solid; yield 80%; mp: 157–161 °C; IR (KBr) $\nu_{max}$: 3440, 3297 (N–H), 3076, 2926, 1722 (C=O), 1677 (C=N), 1624 (C=O), 1577, 1540, 1392, 1243, 1204, 1177, 1124, 1072, 850, 770, 593 $cm^{-1}$; $^1H$ NMR (400 MHz, $CDCl_3$) δ: 10.43 (br s, 1H, 13-NH), 8.96 (s, 1H, 10-H), 7.68 (s, 1H, 8-NH), 7.63 (d, 1H, $J$ = 8.4 Hz, 5-H), 7.35–7.25 (m, 5H, 2′-H, 3′-H, 4′-H, 5′-H, 6′-H), 7.02 (d, 1H, $J$ = 8.4 Hz, 6-H), 6.23 (s, 1H, 3-H), 4.64 (d, 2H, $J$ = 4 Hz, 14-$CH_2$), 2.41 (s, 3H, 11-$CH_3$); $^{13}C$ NMR (100 MHz, $CDCl_3$) δ: 161.5 (C-2), 159.2 (C-8), 156.3 (C-12), 155.4 (C-1a), 152.0 (C-4), 150.9 (C-6a), 138.4 (C-1′), 135.0 (C-10), 128.7 (C-3′,5′), 128.0 (C-5), 127.8 (C-2′,6′), 127.4 (C-4′), 121.1 (C-4a), 115.8 (C-9), 114.0 (C-3), 111.5 (C-10a), 108.5 (C-6), 44.0 (C-14), 18.9 (C-11); ESI-MS *m/z*: 361.1 $[M+H]^+$; HRMS calcd. for $C_{21}H_{17}O_4N_2$: 361.11828, found: 361.11866.

*4.5.9. 8-imino-4-methyl-2-oxo-N-(1-phenylethyl)-2H,8H-pyrano [2,3-f]chromene-9-carboxamide (**6i**)*

Pale yellow solid; yield 66%; mp: 158–160 °C; IR (KBr) $\nu_{max}$: 3444, 3273 (N–H), 3061, 3028, 2969, 2927, 1727 (C=O), 1677 (C=N), 1626 (C=O), 1579, 1550, 1494, 1448, 1389, 1251, 1201, 1062, 823, 770, 701, 598 $cm^{-1}$; $^1H$ NMR (400 MHz, $CDCl_3$) δ: 10.53 (d, 1H, $J$ = 7.2 Hz, 13-NH), 8.96 (s, 1H, 10-H), 7.73 (s, 1H, 8-NH), 7.63 (d, 1H, $J$ = 8.8 Hz, 5-H), 7.41–7.25 (m, 5H, 2′-H, 3′-H, 4′-H, 5′-H, 6′-H), 7.03 (d, 1H, $J$ = 8.8 Hz, 6-H), 6.24 (s, 1H, 3-H), 5.31–5.27 (m, 1H, 14-H), 2.41 (s, 3H, 11-$CH_3$) 1.57 (d, 3H, $J$ = 7.2 Hz, 15-$CH_3$); $^{13}C$ NMR (100 MHz, $CDCl_3$) δ: 160.5 (C-2), 159.1 (C-8), 156.4 (C-12), 155.3 (C-1a), 152.0 (C-4), 150.8 (C-6a), 143.7 (C-1′), 134.8 (C-10), 128.7 (C-3′,5′), 128.0 (C-5), 127.2 (C-4′), 126.3 (C-2′,6′), 121.1 (C-4a), 115.8 (C-9), 114.0 (C-3), 111.5 (C-10a), 108.4 (C-6), 49.6 (C-14), 22.7 (C-15), 18.9 (C-11); ESI-MS *m/z*: 375.2 $[M+H]^+$; HRMS calcd. for $C_{22}H_{19}O_4N_2$: 375.1345, found: 375.1353.

*4.5.10. N9-benzhydryl-8-imino-4-methyl-2-oxo-2H,8H-pyrano [2,3-f]chromene-9-carboxamide (**6j**)*

Pale yellow solid; yield 74%; mp: 174–176 °C; IR (KBr) $\nu_{max}$: 3454, 3317 (N–H), 3201, 3209, 3060, 2925, 1747 (C=O), 1675 (C=N), 1624 (C=O), 1574, 1453, 1389, 1225, 1197, 1067, 832, 760, 596 $cm^{-1}$; $^1H$ NMR (400 MHz, $CDCl_3$) δ: 11.07 (d, 1H, $J$ = 8.4 Hz, 13-NH), 8.91 (s, 1H, 10-H), 7.74 (s, 1H, 8-NH), 7.60 (d, 1H, $J$ = 8.8 Hz, 5-H), 7.35–7.27 (m, 10H, 2′-H, 3′-H, 4′-H, 5′-H, 6′-H and 2″-H, 3″-H, 4″-H, 5″-H, 6″-H), 7.01 (d, 1H, $J$ = 8.8 Hz, 6-H), 6.46 (d, 1H, $J$ = 8.4 Hz, 14-H), 6.20 (s, 1H, 3-H), 2.37 (s, 3H, 11-$CH_3$); $^{13}C$ NMR (100 MHz, $CDCl_3$) δ: 160.7 (C-2), 159.1 (C-8), 156.4 (C-12), 155.4 (C-1a), 152.0 (C-4), 150.8 (C-6a), 142.1 (C-1′,1″), 135.1(C-10), 128.7 (C-3′,5′ and C-3″,5″), 128.1(C-5), 127.5 (C-2′,6′ and C-2″, 6″), 127.0 (C-4′,4″), 121.0 (C-4a), 115.8 (C-9), 114.0 (C-3), 111.5 (C-10a), 108.4 (C-6), 57.5 (C-14), 18.91 (C-11); ESI-MS *m/z*: 437.1 $[M+H]^+$; HRMS calcd. for $C_{27}H_{21}O_4N_2$: 437.14958, found: 437.14966.

*4.5.11. N9-[1-(4-methoxyphenyl)ethyl]-8-imino-4-methyl-2-oxo-2H,8H-pyrano[2,3-f]chromene-9 carboxamide (**6k**)*

Pale yellow solid; yield 80%; mp: 139–142 °C; IR (KBr) $\nu_{max}$: 3447, 3280 (N–H), 3272, 3182, 3094, 3034, 2972, 2930, 2835, 1728 (C=O), 1675 (C=N), 1626 (C=O), 1578, 1446, 1390, 1355, 1201, 1175, 1062, 831, 770, 596 $cm^{-1}$; $^1H$ NMR (400 MHz, $CDCl_3$) δ: 10.44 (d, 1H, $J$ = 7.6 Hz, 13-NH), 8.91 (s, 1H, 10-H), 7.70 (s, 1H, 8-NH), 7.61 (d, 1H, $J$ = 8.8 Hz, 5-H), 7.32 (d, 2H, $J$ = 8.8 Hz, 2′-H, 6′-H), 7.01 (d, 1H, $J$ = 8.8 Hz, 6-H), 6.87 (d, 2H, $J$ = 8.8 Hz, 3′-H, 5′-H), 6.22 (s, 1H, 3-H), 5.25–5.21 (m, 1H, 14-H), 3.78 (s, 3H, 4′-$OCH_3$), 2.40 (s, 3H, 11-$CH_3$), 1.55 (d, 3H, $J$ = 6.8 Hz, 15-$CH_3$); $^{13}C$ NMR (100 MHz, $CDCl_3$) δ: 160.5 (C-2), 159.2 (C-8), 158.7 (C-12), 156.4 (C-4′), 155.4 (C-1a), 152.0 (C-4), 150.8 (C-6a), 135.9 (C-1′), 134.8 (C-10), 128.0 (C-5), 127.4 (C-2′, C-6′), 121.2 (C-4a), 115.8 (C-9), 114.0 (C-3′,5′), 114.0 (C-3), 111.5 (C-10a), 108.5 (C-6), 55.4 (4′-$OCH_3$), 48.9 (C-14), 22.6 (C-15), 18.9 (C-11); ESI-MS *m/z*: 405.2 $[M+H]^+$; HRMS calcd. for $C_{23}H_{21}O_5N_2$: 405.14450, found: 405.14473.

*4.5.12. N-(2,4-dimethoxybenzyl)-8-imino-4-methyl-2-oxo-2H,8H-pyrano[2,3-f]chromene-9-carboxamide (**6l**)*

Brick red solid; yield 81%; mp: 152–155 °C; IR (KBr) $\nu_{max}$: 3447, 3297 (N–H), 3086, 2935, 1740 (C=O), 1675 (C=N), 1626 (C=O), 1578, 1389, 1347, 1225, 1198, 1069, 834, 768, 596 $cm^{-1}$; $^1H$ NMR (400 MHz, $CDCl_3$) δ: 10.34 (t, 1H, $J$ = 5.6 Hz, 13-NH), 8.89 (s, 1H, 10-H), 7.67 (s, 1H, 8-NH), 7.59 (d, 1H, $J$ = 8.8 Hz, 5-H), 7.24 (s, 1H, 3′-H), 6.98 (d, 1H, $J$ = 8.8 Hz, 6-H), 6.46–6.42 (m, 2H, 5′-H, 6′-H), 6.21 (s, 1H, 3-H), 4.55 (d, 2H, $J$ = 5.6 Hz, 14-$CH_2$), 3.84 (s, 3H, 4′-$OCH_3$), 3.78 (s, 3H, 2′-$OCH_3$), 2.40 (s, 3H, 11-$CH_3$); $^{13}C$ NMR (100 MHz, $CDCl_3$) δ: 161.1 (C-2), 160.4 (C-8), 159.2 (C-12), 158.7 (C-4′), 156.2 (C-2′), 155.4 (C-6a), 152.1 (C-4), 150.8 (C-1a), 134.5 (C-6′), 130.2 (C-10), 127.9 (C-5), 121.4 (C-1′), 119.1 (C-10a), 115.7 (C-9), 113.9 (C-4a), 111.5 (C-6), 108.5 (C-5′), 103.9 (C-3′), 98.6 (C-6), 55.5 (2′, 4′ –$OCH_3$), 39.1 (C-14), 18.9 (C-11); ESI-MS *m/z*: 421.2 $[M+H]^+$; HRMS calcd. for $C_{23}H_{21}O_6N_2$: 421.13941, found: 421.13980.

*4.5.13. N-(2-bromobenzyl)-8-imino-4-methyl-2-oxo-2H,8H-pyrano [2,3-f]chromene-9 carboxamide (**6m**)*

Orange solid; yield 73%; mp: 207–209 °C; IR (KBr) $\nu_{max}$: 3439, 3309 (N–H), 3209, 3076, 2924, 2853, 1721 (C=O), 1689 (C=N), 1623 (C=O), 1575, 1556, 1441, 1393, 1204, 1025, 771 $cm^{-1}$; $^1H$ NMR (400 MHz, $CDCl_3$) δ: 10.56 (br s, 1H, 13-NH), 9.02 (s, 1H, 10-H), 7.75 (s, 1H, 8-NH), 7.65 (d, 1H, $J$ = 8.8 Hz, 5-H), 7.56 (d, 1H, $J$ = 9.2 Hz, 3′-H), 7.47 (d, 1H, $J$ = 9.2 Hz, 6′-H), 7.29 (t, 1H, $J$ = 7.6 Hz, 4′-H), 7.14 (t, 1H, $J$ = 7.6 Hz, 5′-H), 7.04 (d, 1H, $J$ = 8.8 Hz, 6-H), 6.26 (s, 1H, 3-H), 4.71 (d, 2H, $J$ = 6 Hz, 14-$CH_2$), 2.43 (s, 3H, 11-$CH_3$); $^{13}C$ NMR (100 MHz, DMSO-$d_6$) δ: 161.5 (C-2), 159.2 (C-8), 155.6 (C-12), 154.5 (C-1a), 153.8 (C-4), 150.5 (C-6a), 137.7 (C-1′), 133.0 (C-10), 132.9 (C-3′), 130.5 (C-6′), 129.9 (C-4′), 128.7 (C-5), 128.3 (C-5′), 123.2 (C-2′), 120.8 (C-4a), 115.7 (C-9), 113.3 (C-3), 111.7 (C-10a), 109.2 (C-6) 43.8 (C-14), 18.7 (C-11); ESI-MS *m/z*: 439.1 $[M+H]^+$; HRMS calcd. for $C_{21}H_{16}BrO_4N_2$: 439.0294, found: 439.0298.

*4.5.14. N-(3-bromobenzyl)-8-imino-4-methyl-2-oxo-2H,8H-pyrano [2,3-f]chromene- 9- carboxamide (**6n**)*

Orange solid; yield 68%; mp: 188–190 °C; IR (KBr) $\nu_{max}$: 3448, 3300 (N–H), 3206, 3062, 2923, 1726 (C=O), 1678 (C=N), 1625 (C=O), 1574, 1589, 1428, 1389, 1199, 1071, 771 $cm^{-1}$; $^1H$ NMR (400 MHz, $CDCl_3$) δ: 10.49 (t, 1H, $J$ = 11.2 Hz, 13-NH), 8.89 (s, 1H, 10-H), 7.71 (s, 1H, 8-NH), 7.63 (d, 1H, $J$ = 8.8 Hz, 5-H), 7.48 (s, 1H, 2′-H), 7.37 (d, 1H, $J$ = 7.6 Hz, 4′-H), 7.27 (d, 1H, $J$ = 7.6 Hz, 6′-H), 7.19 (t, 1H, $J$ = 7.6 Hz, 5′-H), 7.01 (d, 1H, $J$ = 8.8 Hz, 6-H), 6.22 (s, 1H, 3-H), 4.59 (d, 2H, $J$ = 5.6 Hz, 14- $CH_2$), 2.40 (s, 3H, 11-$CH_3$); $^{13}C$ NMR (100 MHz, $CDCl_3$) δ: 161.7 (C-2), 159.1 (C-8), 156.2 (C-12), 155.4 (C-1a), 152.1 (C-4), 150.8 (C-6a), 140.8 (C-1′), 135.1 (C-10), 130.7 (C-2′), 130.4 (C-4′), 130.2 (C-5′), 128.2 (C-5), 126.4 (C-6′), 122.7 (C-3′), 120.8 (C-4a), 115.8 (C-9), 114.0 (C-3), 111.5 (C-10a), 108.3 (C-6) 43.2 (C-14), 18.9 (C-11); ESI-MS *m/z*: 439.1 $[M+H]^+$; HRMS calcd. for $C_{21}H_{16}BrO_4N_2$: 439.0294, found: 439.0300.

*4.5.15. N-(2-chlorobenzyl)-8-imino-4-methyl-2-oxo-2H,8H-pyrano [2,3-f]chromene- 9-carboxamide (**6o**)*

Orange solid; yield 81%; mp: 204–206 °C; IR (KBr) $\nu_{max}$: 3443, 3316 (N–H), 3074, 2925, 2854, 1721 (C=O), 1689 (C=N), 1624 (C=O), 1576, 1556, 1443, 1204, 1058, 771 $cm^{-1}$; $^1H$ NMR (400 MHz, $CDCl_3$) δ: 10.55 (br s, 1H, 13-NH), 9.02 (s, 1H, 10-H), 7.75 (s, 1H, 8-NH), 7.64 (d, 1H, $J$ = 8.8 Hz, 5-H), 7.46 (d, 1H, $J$ = 9.2 Hz, 3′-H), 7.37 (d, 1H, $J$ = 9.2 Hz, 6′-H), 7.24–7.19 (m, 2H, 4′-H, 5′-H), 7.04 (d, 1H, $J$ = 8.8 Hz, 6-H), 6.26 (s, 1H, 3-H), 4.73 (d, 2H, $J$ = 6.0 Hz, 14-$CH_2$), 2.43 (s, 3H, 11-$CH_3$); $^{13}C$ NMR (100 MHz, DMSO-$d_6$) δ: 161.6 (C-2), 159.7 (C-8), 159.1(C-12), 155.5 (C-1a), 153.7 (C-4), 150.4 (C-

6a), 136.1 (C-1′), 132.8 (C-10), 132.2 (C-2′), 130.9 (C-3′), 129.9 (C-6′), 129.7 (C-5), 129.4 (C-4′), 127.8 (C-5′), 120.7 (C-4a), 115.7 (C-9), 113.3 (C-3), 111.6 (C-10a), 109.2 (C-6) 46.2 (C-14), 18.6 (C-11); ESI-MS *m/z* 395.2; $[M+H]^+$; HRMS calcd. for $C_{21}H_{16}ClO_4N_2$: 395.0799, found: 395.0804.

#### 4.5.16. N-(3-chlorobenzyl)-8-imino-4-methyl-2-oxo-2H,8H-pyrano [2,3-f]chromene- 9-carboxamide (**6p**)

Orange solid; yield 65%; mp: 186–188 °C; IR (KBr) $\nu_{max}$: 3444, 3312 (N–H), 3210, 3075, 2924, 2855, 1725 (C=O), 1683 (C=N), 1624 (C=O), 1576, 1556, 1431, 1390, 1201, 1073, 771 $cm^{-1}$; $^1H$ NMR (400 MHz, $CDCl_3$) δ: 10.49 (t, 1H, $J$ = 11.2 Hz, 13-NH), 8.88 (s, 1H, 10-H), 7.71 (s, 1H, 8-NH), 7.63 (d, 1H, $J$ = 8.8 Hz, 5-H), 7.32 (s, 1H, 2′-H), 7.27–7.20 (m, 3H, 4′–6′-H), 7.01 (d, 1H, $J$ = 8.8 Hz, 6-H), 6.21 (s, 1H, 3-H), 4.60 (d, 2H, $J$ = 6.0 Hz, 14-$CH_2$), 2.40 (s, 3H, 11-$CH_3$); $^{13}C$ NMR (100 MHz, $CDCl_3$) δ: 161.7 (C-2), 159.1 (C-8), 156.2 (C-12), 155.3 (C-1a), 152.1(C-4), 150.8 (C-6a), 140.6 (C-1′), 135.0 (C-10), 134.5 (C-3′), 129.9 (C-2′), 128.2 (C-5), 127.7 (C-6′), 127.5 (C-4′), 125.9 (C-5′), 120.7 (C-4a), 115.8 (C-9), 113.9 (C-3), 111.5 (C-10a), 108.3 (C-6), 43.3 (C-14), 18.9 (C-11); ESI-MS *m/z*: 395.2 $[M+H]^+$; HRMS calcd. for $C_{21}H_{16}ClO_4N_2$: 395.0799, found: 395.0809.

#### 4.5.17. N-(4-(tert-butyl)benzyl)-8-imino-4-methyl-2-oxo-2H,8H-pyrano[2,3-f]chromene-9-carboxamide (**6q**)

Pale yellow solid; yield 65%; mp: 216–218 °C; IR (KBr) $\nu_{max}$: 3447, 3302 (N–H), 3075, 3048, 2926, 2958, 1743 (C=O), 1677 (C=N), 1624 (C=O), 1575, 1540, 1201, 1069, 770 $cm^{-1}$; $^1H$ NMR (400 MHz, $CDCl_3$) δ: 10.41 (t, 1H, $J$ = 9.6 Hz, 13-NH), 8.99 (s, 1H, 10-H), 7.70 (s, 1H, 8-NH), 7.64 (d, 1H, $J$ = 8.8 Hz, 5-H), 7.49 (d, 2H, $J$ = 8.4 Hz, 2′-H, 6′-H), 7.29 (d, 2H, $J$ = 8.4 Hz, 3′-H, 5′-H), 7.03 (d, 1H, $J$ = 8.8 Hz, 6-H), 6.25 (s, 1H, 3-H), 4.62 (d, 2H, $J$ = 5.6 Hz, 14-$CH_2$), 2.42 (s, 3H, 11-$CH_3$), 1.31 (s, 9H, 4′-C($CH_3$)$_3$); $^{13}C$ NMR (100 MHz, $CDCl_3$) δ: 161.5 (C-2), 159.2 (C-8), 156.3 (C-12), 155.4 (C-1a), 152.0 (C-4), 150.9 (C-6a), 150.3 (C-4′), 135.3 (C-1′) 135.0 (C-10), 128.0 (C-5), 127.5 (C-2′) 125.6 (C-3′) 121.1 (C-4a), 115.8 (C-9), 114.0 (C-3), 111.5 (C-10a), 108.5 (C-6), 43.7 (C-14), 34.6 (3′-C($CH_3$)$_3$), 31.4 (3′-C($CH_3$)$_3$), 18.9 (C-11); ESI-MS *m/z*: 417.3 $[M+H]^+$; HRMS calcd. for $C_{25}H_{25}O_4N_2$: 417.1815, found: 417.1825.

#### 4.5.18. N9-[2-(2-methoxyphenoxy)ethyl]-8-imino-4-methyl-2-oxo-2H,8H-pyrano[2,3-f]chromene-9-carboxamide (**6r**)

Off white solid; yield 79%; mp: 124–128 °C; IR (KBr) $\nu_{max}$: 3471, 3293 (N–H), 3065, 2953, 2932, 2877, 2839, 1743 (C=O), 1674 (C=N), 1625 (C=O), 1574, 1454, 1388, 1348, 1222, 1196, 819, 769, 596 $cm^{-1}$; $^1H$ NMR (400 MHz, $CDCl_3$) δ: 10.42 (t, 1H, 13-NH), 8.90 (s, 1H, 10-H), 7.78 (s, 1H, 8-NH), 7.63 (d, 1H, $J$ = 8.8 Hz, 5-H), 7.02–6.90 (m, 5H, 6-H, 3′–6′-H), 6.23 (s, 1H, 3-H), 4.21 (m, 2H, 15-$CH_2$), 3.86 (m, 5H, 14- $CH_2$, 2′-$OCH_3$), 2.41 (s, 3H, 11-$CH_3$); $^{13}C$ NMR (100 MHz, $CDCl_3$) δ: 161.9 (C-2), 159.2 (C-8), 156.0 (C-12), 155.4 (C-1a), 152.1 (C-4), 150.8 (C-1′), 150.0 (C-2′), 148.2 (C-6a), 134.7 (C-10), 128.0 (C-5), 121.9 (C-4′), 121.1 (C-5′), 121.1 (C-3′), 115.7 (C-4a), 114.8 (C-9), 113.9 (C-3), 112.4 (C-10a), 111.5 (C-6′), 108.4 (C-6), 68.2 (C-15), 56.1 (2′-$OCH_3$), 39.5 (C-14), 18.9 (C-11); ESI-MS *m/z*: 421.2 $[M+H]^+$; HRMS calcd. for $C_{23}H_{21}O_6N_2$: 421.13941, found: 421.13923.

#### 4.5.19. N9-(2-nitrophenyl)-8-imino-4-methyl-2-oxo-2H,8H-pyrano [2,3-f]chromene- 9-carboxamide (**6s**)

Yellow crystal; yield 64%; mp: 81–84 °C; IR (KBr) $\nu_{max}$: 3440, 3295 (N–H), 3061, 2951, 2877, 1743 (C=O), 1673 (C=N), 1630 (C=O), 1573, 1452, 1385, 1346, 1205, 1192, 820, 767, 595 $cm^{-1}$; $^1H$ NMR (400 MHz, $CDCl_3$) δ: 10.61 (br s, 1H, 13-NH), 8.43 (d, 1H, $J$ = 8.0 Hz, 3′-H), 8.35 (m, 3H, 8-NH, 10-H, 6′-H), 7.72 (d, 1H, $J$ = 8.8 Hz, 5-H), 6.90 (d, 1H, $J$ = 8.8 Hz, 6-H), 6.74 (m, 2H, 4′-H, 5′-H), 6.20 (s, 1H, 3-H), 2.42 (s, 1H, 11-$CH_3$); $^{13}C$ NMR (100 MHz, $CDCl_3$) δ: 168.1 (C-2), 167.9 (C-8), 164.9 (C-12), 164.5 (C-1a), 161.8 (C-4), 159.6 (C-6a), 153.4 (C-2′), 143.4 (C-5′), 143.2 (C-1′), 132.8 (C-10), 128.6 (C-6′), 128.4 (C-5), 115.6 (C-4a), 115.5 (C-3′), 115.3 (C-4′), 115.0(C-9), 113.3 (C-3), 113.1 (C-10a), 109.4 (C-6), 18.6 (C-11); ESI-MS *m/z*: 392.1 $[M+H]^+$; HRMS calcd. for $C_{20}H_{14}O_4N_2$: 392.1026, found: 392.1028.

### 4.6. Biological assays

#### 4.6.1. Determination of AChE and BuChE inhibitory activities

Inhibitory potency of target compounds against AChE and BuChE were assayed using spectrophotometric method developed by Ellman et al. with slight modification [37,38]. *Ee*AChE (EC. 3.1.1.7, Electric eel) *Eq*BuChE (EC 3.1.1.8, horse serum), DTNB, ATC and BTC iodide were purchased from Sigma Aldrich, USA. In brief, reaction mixture composed of 10 μL of test sample of five different concentrations (0.2, 0.4, 0.6, 0.8 and 1.0 μM for AChE assay; 15, 30, 60, 90, 120 μM for BuChE assay), 145 μL phosphate buffer 200 mM (pH 7.7), 80 μL of dithiobisnitrobenzoic acid (DTNB) (18.5 mg of DTNB dissolved in 10 mL phosphate buffer pH 7.7), and 10 μL of enzyme (0.4 U/mL). The mixture was incubated at 25 °C for 5 min. Subsequently, the enzymatic reaction was initiated by addition of 15 μL of 1 mM of acetylthiocholine iodide or butyrylthiocholine iodide (according to the respective enzyme) and the mixture was again incubated for 5 min at 25 °C. The rate of absorbance change was measured at 412 nm for 6 min using a microplate reader (Bio-Rad 680). Inhibition percentage was calculated as follows: % inhibition = (E−S)/E × 100, where E is the enzymatic activity without test compound and S is the enzymatic activity with the test compound. The $IC_{50}$ values were determined graphically from inhibition curves (log inhibitor concentration Vs. percent of inhibition).

#### 4.6.2. In vitro antioxidant activity assay

The radical scavenging activity of the test compounds was measured by the ABTS method [39]. The ABTS was dissolved in water to obtain an 8 mM concentration of ABTS stock solution. ABTS radical cation ($ABTS^{\bullet+}$) was generated by adding 3 mM potassium persulfate to the ABTS stock solution and keeping it in the dark at room temperature for 12–18 h. The $ABTS^{\bullet+}$ solution was diluted with ethanol to give an absorbance of 0.48 ± 0.07 at 734 nm. The 10 μL of the test compounds were allowed to react with 290 μL of $ABTS^{\bullet+}$ solution. The absorbance was taken 30 min after initial mixing. Trolox was used as a standard.

#### 4.6.3. Cell culture, treatment and cell viability (MTT) assay

SK N SH, human neuroblastoma cells were obtained from National Centre for Cell Sciences (Pune, India). The cells were cultured in MEM containing 0.5 mM L-glutamine, 0.1 mM sodium pyruvate and 1 mM non-essential amino acids with 10% FBS in a highly humidified atmosphere having 5% $CO_2$ at 37 °C. Cell cultures at approximately 80% confluence were used for all *in vitro* experimental procedures.

*4.6.3.1. Measurement of cell viability by MTT assay.* Cytotoxic effects of selected compounds (**6m**, **6n**, **6o**, **6p** and **6q**) on the cell viability was measured by using MTT assay as described in our previous studies [40,41]. SK N SH cells ($0.2 \times 10^6$ cells per well) in 200 μL of corresponding medium with 10% FBS were seeded into 96-wellplate. Increasing concentrations of compounds or galantamine dissolved in DMSO were added to the cells and incubated at 37 °C for 24 h in a humidified $CO_2$ incubator with 5% $CO_2$. The medium was replaced along with 20 μL of 5 mg/mL MTT (3-(4, 5-dimethylthiozol-2-yl)-2,5-diphenyltetrazoliumbromide). It was further incubated for 4 h in humidified atmosphere, the medium was removed and 200 μL of 0.1 N acidic isopropyl alcohol was added to the wells to dissolve the MTT formazan crystals. Absorbance was recorded at 570 nm immediately after the development

of purple color. Relative cell viability was evaluated according to the quantity of MTT converted into insoluble formazan salt. The optical density of the formazan generated in the control cells was considered to represent 100% viability. The results were expressed as mean percent of viable cells versus respective control. Experiments were repeated three times and the results represented as averages with standard error.

*4.6.3.2. Protection against $H_2O_2$ induced cell death in SK N SH cell.* Neuroprotective effect of selected compounds (**6m**, **6n**, **6o**, **6p** and **6q**) against $H_2O_2$ induced oxidative injury in SK N SH cells was determined [40,41]. Thus, SK N SH cells were pretreated with different concentrations of compounds (40–120 μM) and galantamine as reference compound for 3 h before treatment with $H_2O_2$ (1.0 mM). $H_2O_2$ was added to the medium to induce oxidative stress and incubated for 24 h in humidified atmosphere. The cell viability was measured by MTT colorimetry as described above.

### 4.7. Kinetic study

To obtain estimates of the inhibition model and inhibition constant Ki, reciprocal plots of 1/V versus 1/[S] were constructed at different concentrations of the substrate acetylthiocholine iodide (0.1–0.5 mM) by using Ellman's method [42]. The assay solution (250 μL) consists of 145 μL of 200 mM phosphate buffer (pH 7.7), with the addition of 80 μL of DTNB (18.5 mg of DTNB dissolved in 10 mL phosphate buffer pH 7.7), 10 μL of 0.4 units/mL AChE, and 15 μL of substrate (ATCh). Three different concentrations of inhibitors (0.002, 0.005 and 0.02 μM) were added to the assay solution and pre-incubated for 5 min at 25 °C with the AChE followed by the addition of substrate in different concentrations. The parallel control experiments were performed without inhibitor in the assay. Progress curves were monitored at 412 nm over 6 min. Then, double reciprocal plots (1/v Vs. 1/[s]) were constructed using Graph pad prism version 5. The re-plots of the slopes and intercepts of the double reciprocal plots against inhibitor concentrations gave the inhibitor constants ($K_{i1}$ and $K_{i2}$, for the binding to free enzyme and enzyme substrate complex) as the intercepts on the x-axis. Data analysis was performed using Microsoft Excel.

### 4.8. Molecular modeling study

To predict the binding modes of target compounds in the active sites of AChE and BuChE enzymes, molecular docking studies were performed using Schrödinger maestro software (version 9.2; Schrödinger LLC, NewYork). The proteins used for docking are the crystal structure of Electric eel acetyl cholinesterase (PDB ID: 1C2O) and the predicted 3D model of horse butyrylcholinesterase [43]. The results were characterized by the G Scores obtained from GLIDE (Grid-based Ligand Docking with Energetics) docking [44].

#### 4.8.1. Protein preparation

Prior to docking, proteins were prepared using protein preparation wizard. Hydrogen atoms were added to the proteins and charges were assigned. Water molecules and other heteroatoms were excluded from the crystal structure as they were not significant for the proteins function. Subsequently, the proteins were optimized and energy minimized using OPLS2005 force field. A grid was generated around the active site of the enzyme by specifying the key active site residues reported in the literature using GLIDE module of Schrodinger.

#### 4.8.2. Ligand preparation

The ligands used as inputs for docking were designed using ChemBioOffice 2010 software and prepared using LigPrep (version 2.5, Schrödinger Inc.). Preparation of ligands includes assigning bond orders, generating various tautomers, ring conformations and stereo chemistries. All the conformations generated were minimized using OPLS-AA force field before proceeding for docking studies.

#### 4.8.3. Receptor grid generation

A receptor grid was generated around the protein active site by choosing the residues D74, T83, W86, G120, G121, G122, Y124, Y133, E202, S203, W286, F295, F297, Y337, and Y341 reported in the literature. Grid box size was set at 20 Å × 20 Å × 20 Å and Vander Waal radii of receptor atoms were scaled to 1.00 Å with a partial atomic charge of 0.25.

#### 4.8.4. Docking

Glide module of Schrodinger was used for the docking studies. All docking calculations were performed using Standard Precision (SP) mode. A scaling factor of 0.8 and a partial atomic charge of less than 0.15 was applied to the atoms of the protein. The poses generated per ligand were set to 10,000 and the pose chosen for energy minimization was set to 10. Glide docking score was used to determine the best docked structure from the output. The interactions of these docked complexes were investigated further.

### 4.9. In vivo brain AChE activity assay

#### 4.9.1. Animals

Sixteen adult male BALB/c ByJ mice were used in this study. They were kept in the Central Animal House facility of Sri Venkateswara University, Tirupati, India. The animals were housed in a propylene cages in a room maintained at 25 °C, 45–50% relative humidity under a 12 h light/dark cycle with *ad libitum* access to standard rodent pellet diet and water. All experimental procedures involving the animals were performed in accordance with the Animal Ethics Committee of Sri Venkateswara University (No. 55/2012/(i)/a/CPCSEA/IAEC/SVU/MBJ, dated 08-07-2012), Tirupati, approved by the Government of India.

#### 4.9.2. Drug adminstrattion

Compound 6n was dissolved in DMSO and administered through intraperitoneal injection at doses ranging from 16 to 200 mg/kg, this method ensured better drug absorption by the mice, compared to oral administration.

#### 4.9.3. Tissue preparation for bioassay

After 48 h of intraperitoneal injection, animals were sacrificed under deep anaesthesia with ether and their brains were taken out quickly and perfused in situ with 0.15 M NaCl until free of blood and then removed into 0.2 M phosphate buffer, pH 7.7. Dissected brain was homogenized in 200 mM phosphate buffer (pH 7.7) having 10 μL/mL protease inhibitor to get 5% (w/v) homogenate. The homogenate was centrifuged at 10,000 × *g* for 10 min at 4 °C to separate the nuclear debris. The supernatant thus obtained was used for the estimation of activity of acetylcholine esterase. The brain acetylcholinesterase activity at different volumes of supernatant (10, 20, 30, 40 and 50 μL) with 15 μL of 1 mM ATCh was determined using Ellman method.

## Acknowledgments

This work was supported by start-up grant (SR/FT/CS-60/2010) from Department of Science and Technology (DST), New Delhi, India. The authors thank Department of Chemistry, Pondicherry

University for providing ESI HRMS spectra from DST FIST facility and Dr. K.S.V. Krishna Rao for providing IR instrumental facility. We are appreciated for the help and support of Dr. M. Balaji in animal experiments. Authors also thank Dr. R.V.J. Kashyap and Dr. S. Rajagopal for critical reading and improving the manuscript.

## Appendix A. Supplementary data

Supplementary data related to this article can be found at http://dx.doi.org/10.1016/j.ejmech.2015.10.046.

## References

[1] W. Xing, Y. Fu, Z. Shi, D. Lu, H. Zhang, Y. Hu, Discovery of novel 2,6-disubstituted pyridazinone derivatives as acetylcholinesterase inhibitors, Eur. J. Med. Chem. 63 (2013) 95–103.
[2] M. Palmer, Neuroprotective therapeutics for Alzheimer's disease: progress and prospects, Trends Pharmacol. Sci. 32 (2011) 141–147.
[3] M. Citron, Alzheimer's disease: strategies for disease modification, Nat. Rev. Drug Discov. 9 (2010) 387–398.
[4] M. Bartolini, C. Bertucci, V. Cavrini, V. Andrisano, β-Amyloid aggregation induced by human acetylcholinesterase: inhibition studies, Biochem. Pharmacol. 65 (2003) 407–416.
[5] N.C. Inestrosa, A. Alvarez, C.A. Perez, R.D. Moreno, M. Vicente, C. Linker, O.I. Casanueva, C. Soto, J. Garrido, Acetylcholinesterase accelerates assembly of amyloid-β-peptides into Alzheimer's fibrils: possible role of the peripheral site of the enzyme, Neuron 16 (1996) 881–891.
[6] A. Castro, A. Martinez, Peripheral and dual binding site acetylcholinesterase inhibitors: implications in treatment of Alzheimer's disease, Mini Rev. Med. Chem. 1 (2001) 267–272.
[7] E. Giacobini, Cholinesterases: new roles in brain function and in Alzheimer's disease, Neurochem. Res. 28 (2003) 515–522.
[8] M. Pera, A. Martinez-Otero, L. Colombo, M. Salmona, D. Ruiz-Molina, A. Badia, et al., Acetylcholinesterase as an amyloid enhancing factor in PrP82-146 aggregation process, Mol. Cell Neurosci. 40 (2009) 217–224.
[9] H. Soreq, S. Seidman, Acetylcholinesterase e new roles for an old actor, Nat. Rev. Neurosci. 2 (2001) 294–302.
[10] R.S. Li, X.B. Wang, X.J. Hu, L.Y. Kong, Design, synthesis and evaluation of flavonoid derivatives as potential multifunctional acetylcholinesterase inhibitors against Alzheimer's disease, Bioorg. Med. Chem. Lett. 23 (2013), 2636–264.
[11] R.M. Lane, S.G. Potkin, A. Enz, Targeting acetylcholinesterase and butyrylcholinesterase in dementia, Int. J. Neuropsychopharmacol. 9 (2005) 1–24.
[12] D.R. Liston, J.A. Nielsen, A. Villalobos, D. Chapin, S.B. Jones, S.T. Hubbard, I.A. Shalaby, A. Ramirez, D. Nason, W.F. White, Pharmacology of selective acetylcholinesterase inhibitors: implications for use in Alzheimer's disease, Eur. J. Pharmacol. 486 (2004) 9–17.
[13] M.A. Ansari, S.W. Scheff, Oxidative stress in the progression of Alzheimer disease in the frontal cortex, J. Neuropathol. Exp. Neurol. 69 (2010) 155–167.
[14] R. Nunomura, X.J. Castellani, P.I. Zhu, G. Moreira, M.A. Perry, Smith, Involvement of oxidative stress in Alzheimer disease, J. Neuropathol. Exp. Neurol. 65 (2006) 631.
[15] D.X. Tan, L.C. Manchester, R. Sainz, J.C. Mayo, F.L. Alvares, Antioxidant strategies in protection against neurodegenerative disorders, Expert Opin. Ther. Pat. 13 (2003) 1513–1543.
[16] S. Thiratmatrakul, C. Yenjai, P. Waiwut, O. Vajragupta, P. Reubroycharoen, M. Tohda, C. Boonyarat, Synthesis, biological evaluation and molecular modeling study of novel Tacrine-carbazole hybrids as potential multifunctional agents for the treatment of Alzheimer's disease, Eur. J. Med. Chem. 75 (2014) 21–30.
[17] P. Anand, B. Singh, A review on cholinesterase inhibitors for Alzheimer's disease,, Archives Pharmacal Res. 36 (2013) 375–399.
[18] P. Anand, B. Singh, N. Singh, A review on coumarins as acetylcholinesterase inhibitors for Alzheimer's disease, Bioorg. Med. Chem. 20 (2012) 1175–1180.
[19] L. Piazzi, A. Cavalli, F. Colizzi, F. Belluti, M. Bartolini, F. Mancini, M. Recanatini, V. Andrisano, A. Rampa, Multi-target-directed coumarin derivatives: hAChE and BACE1 inhibitors as potential anti-Alzheimer compounds, Bioorg. Med. Chem. Lett. 18 (2008) 423.
[20] C. Garino, N. Pietrancosta, Y. Laras, V. Moret, A. Rolland, G. Quelever, J.L. Kraus, BACE-1 inhibitory activities of new substituted phenyl-piperazine coupled to various heterocycles: chromene, coumarin and quinoline, Bioorg. Med. Chem. Lett. 16 (2006) 1995.
[21] D.D. Soto-Ortega, B.P. Murphy, F.J. Gonzalez-Velasquez, K.A. Wilson, F. Xie, Q. Wang, M.A. Moss, Inhibition of amyloid-β aggregation by coumarin analogs can be manipulated by functionalization of the aromatic center, Bioorg. Med. Chem. 19 (2011) 2596.
[22] C.A. Kontogiorgis, Y. Xu, D. Hadjipavlou-Litina, Y. Luo, Coumarin derivatives protection against ROS production in cellular models of Abeta toxicities, Free Radic. Res. 41 (2007) 1168.
[23] B.Z. Kurt, I. Gazioglu, F. Sonmez, M. Kucukislamoglu, Synthesis, antioxidant and anticholinesterase activities of novel coumarylthiazole derivatives, Bioorg. Chem. 59 (2015) 80–90.
[24] M. Alipour, M. Khoobi, A. Moradi, H. Nadri, F.H. Moghadam, S. Emami, Z. Hasanpour, A. Foroumadi, A. Shafiee, Synthesis and anti-cholinesterase activity of new 7- hydroxycoumarin derivatives, Eur. J. Med. Chem. 83 (2014) 536–544.
[25] A. Asadipour, M. Alipour, M. Jafari, M. Khoobi, S. Emami, H. Nadri, A. Sakhteman, A. Moradi, V. Sheibani, F.H. Moghadam, A. Shafiee, A. Foroumadi, Novel coumarin-3 carboxamides bearing N-benzylpiperidine moiety as potent acetylcholinesterase inhibitors, Eur. J. Med. Chem. 70 (2013) 623–630.
[26] M. Catto, L. Pisani, F. Leonetti, O. Nicolotti, P. Pesce, A. Stefanachi, S. Cellamare, A. Carotti, Design, synthesis and biological evaluation of coumarin alkylamines as potent and selective dual binding site inhibitors of acetylcholinesterase, Bioorg. Med. Chem. 21 (2013) 146–152.
[27] M. Alipour, M. Khoobi, A. Foroumadi, H. Nadri, A. Moradi, A. Sakhteman, M. Ghandi, A. Shafiee, Novel coumarin derivatives bearing N-benzyl pyridinium moiety: potent and dual binding site acetylcholinesterase inhibitors, Bioorg. Med. Chem. 20 (2012) 7214–7222.
[28] S.F. Razavi, M. Khoobi, H. Nadri, A. Sakhteman, A. Moradi, S. Emami, A. Foroumadi, A. Shafiee, Synthesis and evaluation of 4-substituted coumarins as novel acetylcholinesterase inhibitors, Eur. J. Med. Chem. 64 (2013) 252–259.
[29] M. Khoobi, M. Alipour, A. Moradi, A. Sakhteman, H. Nadri, S.F. Razavi, M. Ghandi, A. Foroumadi, A. Shafiee, Design, synthesis, docking study and biological evaluation of some novel tetrahydrochromeno [3′,4′:5,6]pyrano [2,3-b]quinolin-6(7H)-one derivatives against acetyl- and butyrylcholinesterase, Eur. J. Med. Chem. 68 (2013) 291–300.
[30] L. Piazzi, A. Cavalli, F. Colizzi, F. Belluti, M. Bartolini, F. Mancini, et al., Multi-target- directed coumarin derivatives: hAChE and BACE1 inhibitors as potential anti-Alzheimer compounds, Bioorg. Med. Chem. Lett. 18 (2008) 423–426.
[31] M. Khoobi, M. Alipour, A. Sakhteman, H. Nadri, A. Moradi, M. Ghandi, S. Emami, A. Foroumadi, A. Shafiee, Design, synthesis, biological evaluation and docking study of 5- oxo- 4,5-dihydropyrano[3,2-c]chromene derivatives as acetylcholinesterase and butyrylcholinesterase inhibitors, Eur. J. Med. Chem. 68 (2013) 260–269.
[32] K. Wang, K. Nguyen, Y. Huang, A. Domling, Cyanoacetamide multicomponent reaction (I): parallel synthesis of cyanoacetamides, J. Comb. Chem. 11 (2009) 920.
[33] P. Tamiz, S.X. Cai, Z.L. Zhou, P.W. Yuen, R.M. Schelkun, E.R. Whittemore, E. Weber, R.M. Woodward, J.F.W. Keana, Structure-activity relationship of N-(phenylalkyl)cinnamides as novel NR2B subtype-selective NMDA receptor antagonists, J. Med. Chem. 42 (1999) 3412.
[34] H. Pechmann, C. Duisberg, Ber. die Verbindungen der Phenole mit Acetessigäther Dtsch, Chem. Ges. 16 (1883) 2119.
[35] D.R. Bender, D. Kanne, J.D. Frazier, H. Rapoport, Synthesis and derivitization of 8- acetylpsoralens. Acetyl migrations during Claisen rearrangement, J. Org. Chem. 48 (1983) 2709–2719.
[36] J. Volmajer, R. Toplak, I. Lebanb, A.M. Le Marechala, Synthesis of new iminocoumarins and their transformations into N-chloro and hydrazono compounds, Tetrahedron 61 (2005) 7012–7021.
[37] G.L. Ellman, K.D. Courtney, V. Andres Jr., R.M. Featherstone, A new and rapid colorimetric determination of acetylcholinesterase activity, Biochem. Pharmacol. 7 (1961) 88–95.
[38] H. Nadri, M. Pirali-Hamedani, M. Shekarchi, M. Abdollahi, V. Sheibani, M. Amanlou, et al., Design, synthesis and anticholinesterase activity of a novel series of 1-benzyl-4-((6-alkoxy-3-oxobenzofuran-2(3H)-ylidene) methyl) pyridinium derivatives, Bioorg. Med. Chem. 18 (2010) 6360–6366.
[39] N.J. Miller, C.A. Rice-Evans, Factors influencing the antioxidant activity determined by the $ABTS^{d+}$ radical cation assay, Free Radic. Res. 26 (1997) 195–199.
[40] V. Ramakrishna, K. Preeti Gupta, H. Oruganti Setty, K. Anand Kondapi, Neuroprotective effect of *Emblica Officinalis* extract against $H_2O_2$ induced DNA damage and repair in neuroblastoma cells, J. Homeop. Ayurv. Med. S1002 (2014) 1–5.
[41] M. Valko, D. Leibfritz, J. Moncol, M.T. Cronin, M. Mazur, et al., Free radicals and antioxidants in normal physiological functions and human disease, Int. J. Biochem. Cell Biol. 39 (2007) 44–84.
[42] A. Rampa, F. Bisi, S. Belluti, P. Gobbi, V. Valenti, V. Andrisano, A. Cavrini, M. Cavalli, Recanatini, acetylcholinesterase inhibitors for potential use in Alzheimer's disease: molecular modeling, synthesis and kinetic evaluation of 11H-indeno-[1,2-b]-quinolin-10- ylamine derivatives, Bioorg. Med. Chem. 8 (2000) 497–506.
[43] Y. Bourne, et al., Conformational flexibility of the acetylcholinesterase tetramer suggested by X-ray crystallography, J. Biol. Chem. 43 (1999) 370–376.
[44] R.A. Friesner, et al., *Glide*: a new approach for rapid, accurate docking and scoring. 1. Method and assessment of docking accuracy, J. Med. Chem. 47 (2004) 1739–1749.
[45] Rapid ADME, QikProp, Version 3.5, Schrödinger, LLC, New York, NY, 2012.
[46] H. Pajouhesh, G.R. Lenz, Medicinal chemical properties of successful central nervous system drugs, NeuroRx 4 (2005) 541–553.
[47] D.E. Clark, S.D. Pickett, Computational methods for the prediction of 'drug-likeness', Drug. Discov. Today 2 (2000) 49–58.

[48] C.A. Lipinski, F. Lombardo, B.W. Dominy, P.J. Feeney, Experimental and computational approaches to estimate solubility and permeability in drug discovery and development settings, Adv. Drug. Deliv. Rev. 46 (2001) 3–26.

[49] F. Hobbiger, R. Landaster, Determination of acetylcholinesterase activity of brain slices and its significance in studies of extracellular acetylcholinesterase, J. Neurochem. 18 (1971) 1741–1749.